
TOWARDS LARGE-SCALE IN-CONTEXT REINFORCEMENT LEARNING BY META-TRAINING IN RANDOMIZED WORLDS

*†Fan Wang^{1,2}, *Pengtao Shao¹, Yiming Zhang¹, Bo Yu¹, †Shaoshan Liu¹,
Ning Ding¹, Yang Cao², Yu Kang², and Haifeng Wang³

¹Shenzhen Institute of Artificial Intelligence and Robotics for Society, Shenzhen, China

²University of Science and Technology of China, Shenzhen, China

³Baidu Inc, Beijing, China

July 2, 2025

ABSTRACT

In-Context Reinforcement Learning (ICRL) enables agents to learn automatically and on-the-fly from their interactive experiences. However, a major challenge in scaling up ICRL is the lack of scalable task collections. To address this, we propose the procedurally generated tabular Markov Decision Processes, named AnyMDP. Through a carefully designed randomization process, AnyMDP is capable of generating high-quality tasks on a large scale while maintaining relatively low structural biases. To facilitate efficient meta-training at scale, we further introduce step-wise supervision and induce prior information in the ICRL framework. Our results demonstrate that, with a sufficiently large scale of AnyMDP tasks, the proposed model can generalize to tasks that were not considered in the training set. The scalable task set provided by AnyMDP also enables a more thorough empirical investigation of the relationship between data distribution and ICRL performance. We further show that the generalization of ICRL potentially comes at the cost of increased task diversity and longer adaptation periods. This finding carries critical implications for scaling robust ICRL capabilities, highlighting the necessity of diverse and extensive task design, and prioritizing asymptotic performance over few-shot adaptation.

1 Introduction

Large-scale pre-training has achieved tremendous success, especially in processing natural languages, images, and videos [1–4]. They have demonstrated the ability to address unseen tasks through *in-context learning* (ICL) [5], a paradigm that leverages contextual information to enhance performance. Unlike *in-weight learning* (IWL), which relies on gradient-based updates to model weights, ICL enables models to acquire new skills in a few-shot manner, thereby enhancing their adaptability to novel environments. Sharing commonalities with model-based meta-learning approaches [6, 7], ICL can accommodate traditional learning paradigms within its framework, including supervised learning [7, 8], imitation learning [9–11], and reinforcement learning [12–15]. This significantly alleviates the need for laborious human-designed objective functions and optimization strategies, which are typically required in IWL. Further, gradient-based IWL has been criticized for its inefficiency in continuously adapting to new tasks [16]. In contrast, ICL has demonstrated plasticity that resembles the adaptability of the human brain [17].

On the one hand, pre-training on massive uncurated data faces limitations in terms of the controllability of ICL. The mechanisms underlying the emergence of ICL capabilities and their limitations are not yet fully understood [18]. Additionally, the robustness of ICL in pre-training is under question [19]. On the other hand, meta-learning aims to develop in-context learning functionality rather than master specific skills. However, the efficacy of these approaches is frequently constrained by the scarcity of large, diverse datasets and the narrow scope of available tasks—limitations

*Equal Contribution

†Corresponding to: wangfan@cuhk.edu.cn, shaoshanliu@cuhk.edu.cn

particularly pronounced in meta-reinforcement learning (MetaRL) and in-context reinforcement learning (ICRL). Consequently, most existing studies evaluate a model’s adaptive capacity solely within narrowly defined domains, thereby restricting the broader generalization of these methods.

To further enhance the scalability and generality of ICRL, we extend the widely used multi-armed bandit benchmark [20] to tabular Markov Decision Processes (MDPs). We introduce AnyMDP, a scalable task generation framework where MDPs are designed with fully randomized transition and reward functions. To produce non-trivial environments with minimal structural bias, we propose a procedural generation method that synthesizes diverse tasks, creating significant challenges for learners. To scale ICRL efficiently, we further enhance the modeling and training framework with two key innovations: *step-wise supervision* and *prior knowledge induction*. This allows us to meta-train models on an unprecedented scale—over 6 billion time steps and context lengths exceeding 512K. The model, referred to as *OmniRL*, was trained exclusively on AnyMDP tasks and demonstrated robust generalization to entirely unseen Gymnasium environments. This serves to validate the efficacy of the framework. Using the scalable task set, we further investigate how data distribution impacts ICRL performance at scale. Our experiments reveal three critical insights: (1) data coverage and extensiveness are crucial for effective meta-learning, as these factors delineate the boundaries between IWL-dominated task identification and ICL-dominated general-purpose learning paradigms; and (2) asymptotic performance (i.e., long-term adaptation) can be a more reliable indicator of ICRL capability than zero-shot or few-shot performance metrics; (3) there is considerable potential for training regimes that prioritize task diversity and extensiveness, over fidelity to prior experiences.

To summarize, our contributions includes: (1) We introduce AnyMDP, a scalable tabular MDP generation framework designed to support the training of ICRL on over 100K tasks across tens of billions of simulation steps. In addition, we propose an efficient training and model framework for ICRL that ensures scalability. (2) We examine how data distribution affects ICRL and empirically verify the need for diverse and extensive task design, along with the importance of evaluating asymptotic performance.

2 Related Work

2.1 Emergence of In-Context Learning

Meta-learning, also known as learning to learn [21], pertains to a category of approaches that prioritize the acquisition of generalizable adaptation skills across a spectrum of tasks. It encompasses a broad array of methodologies, including gradient-based optimization [22] and model-based meta-learning [6]. Meta-learning concepts align with the formation of System 3 [23], which involves synaptic recalibration for environmental adaptation and complementing LLMs’ System 1 (intuitive thinking) and System 2 (in-context reasoning). Large models pre-trained with huge, uncensored datasets also incentivize ICL in a manner similar to meta-learning [5, 9, 24–28]. For clarity, "pre-training" describes training targeting skill acquisition, typically followed by gradient-based tuning, while "meta-training" refers to training for acquiring learning ability without requiring subsequent gradient-based tuning. Numerous theoretical investigations [19, 29–31] have been conducted to rigorously uncover the association between ICL ability and pre-training data distribution. Empirical evidence demonstrates that burstiness significantly enhances ICL performance in both language modeling tasks [30] and decision-making problems [26]. Current ICL implementations predominantly function as few-shot learners [32, 33], particularly in scenarios with insufficient task diversity. Analyses and experiments have been conducted to show that computation-based ICL can exhibit a richer array of behaviors than gradient-based IWL [34–36], particularly in terms of plasticity and continual learning [17], which makes ICL potentially a generalized learner. However, recent studies indicate that models tend to prioritize reliance on IWL over ICL whenever feasible [31]. Our research aligns with the growing body of work on general-purpose in-context learning [32, 37, 38], which emphasizes ICL as the primary mechanism for skill acquisition rather than IWL.

2.2 In-Context Reinforcement Learning

In-context reinforcement learning (ICRL) encompasses algorithms that dynamically adapt to contextual information by synthesizing self-generated trajectories and incorporating external feedback [6, 12]. It typically employs recurrent neural structures [6] and attention structures [12, 20] that are capable of encoding the historical interactions in the *inner loop*. The meta-training process that optimizes the parameters specifying the learning mechanisms of the inner loop is called *outer loop*. Common choices for the outer-loop optimizer for ICRL include reinforcement learning [6, 13, 20], evolutionary strategies [39, 40], and supervised learning [12, 15]. While supervised learning generally achieves greater sample efficiency compared to RL and evolutionary strategies, it often suffers from weaker regret bounds [41, 42]. Additionally, the absence of an oracle policy—a key requirement for supervised learning—can pose a critical bottleneck. In such cases, frameworks like RL Coaches [9, 43] offer viable alternatives by bridging the gap between supervised

paradigms and reinforcement learning. Another significant challenge in the study of In-context Reinforcement Learning (ICRL) stems from the scarcity of large-scale task sets, as task diversity and scale are critical for ICL ability [44]. Existing research predominantly employs domain randomization techniques to expand canonical reinforcement learning environments into broader classes of related environments. Building general-purpose adaptive agents in an open-ended world has attracted much attention in recent years [37, 45–48]. However, existing environments suffer from significant structural biases, which hinder the direct applicability of ICRL models trained on one task class to another.

2.3 Domain Randomization

Domain Randomization (DR) was originally introduced to improve sim-to-real transfer [49]. In Meta-learning, it is also common to randomize a subset of domain parameters to create these variant tasks. These benchmarks can be typically categorized into randomizing the rewards or targets while keeping the transitions fixed [12, 15, 20, 22, 50, 51], randomizing the dynamics while keeping the targets unchanged [39, 40, 52–54], and randomizing the observations and labels without altering the underlying transitions and rewards [32, 55, 56]. In addition to static rule-based randomization, automatic domain randomization [46, 57] introduces a dynamic randomization process by automatically searching for the best performance in the target domain. Although DR creates a class of tasks with a certain variety, it is restricted by the original task setting. Recently, researchers have proposed generating entirely new tasks through randomization, a method designed to minimize structural biases [38, 58, 59]. This approach represents a promising direction for advancing scalable ICRL with minimum inductive biases.

3 Methodology

3.1 Generating AnyMDP tasks by World Randomization

Motivations. To promote general-purpose ICL, we argue that a critical step is reducing the shared structure (common ground) across tasks in the training set. By reducing dependence on IWL, the trained model will instead rely primarily on ICL to solve specific tasks. This suggests prioritizing task diversity and coverage over fidelity to real-world scenarios, ensuring the model generalizes beyond narrow patterns. Inspired by these advancements, we introduce *world randomization*, which extends beyond traditional domain randomization to further diversify the task set. It is designed to minimize inductive biases in task formulation, thereby further enhancing task diversity and coverage.

Formulations. We denote a task of Markov Decision Processes (MDPs) with $\tau = \langle \mathcal{S}, \mathcal{A}, \mathcal{P}, \mathcal{R}, \mathcal{S}_0, \mathcal{S}_E, T_E, \gamma \rangle$ where \mathcal{S} denotes the state space, \mathcal{A} the action space, $\mathcal{P} : \mathcal{S} \times \mathcal{A} \rightarrow \mathcal{S}$ the state-transition probability distribution, $\mathcal{R} : \mathcal{S} \times \mathcal{A} \times \mathcal{S} \rightarrow \mathbb{R}$ the reward function, \mathcal{S}_0 the set of initial states, and \mathcal{S}_E the set of terminal states, T_E the maximum steps in an episode, and γ the discount factor. We consider only fully visible discrete MDPs with $\mathcal{S} = \{1, \dots, n_s\}$, $\mathcal{A} = \{1, \dots, n_a\}$, denoted by $\tau(n_s, n_a)$. With these notations, domain randomization with base task τ can be represented as $\mathcal{DR}(\tau) = \langle \mathcal{S}, \mathcal{A}, \mathcal{P} + \epsilon_P, \mathcal{R} + \epsilon_R, \mathcal{S}_0, \mathcal{S}_E, T_E \rangle$.

We then formally define the *AnyMDP* task set $\mathcal{T}(n_s, n_a)$, which is constructed through MDPs and world randomization, with $|\mathcal{S}| \leq n_s$ and $|\mathcal{A}| \leq n_a$, as:

$$\mathcal{T}(n_s, n_a) = \{\tau(n_s, n_a) | \mathcal{P}, \mathcal{R}, \mathcal{S}_0, \mathcal{S}_E, T_E \sim \text{Random}\} \quad (1)$$

with $\mathcal{R}(s, a, s') \sim \mathcal{N}(\mu_{\mathcal{R}}(s, a, s'), \Sigma_{\mathcal{R}}(s, a, s'))$, \mathcal{P} , $\mu_{\mathcal{R}}$, and $\Sigma_{\mathcal{R}}$ sampled randomly from $\mathbb{R}^{n_s \times n_a \times n_s}$, $\mathcal{S}_0, \mathcal{S}_E \subset \mathcal{S}$, and $T_E \in [T_{min}, T_{max}]$.

Procedural Generation Algorithm. Although Equation (1) can be used to represent any tasks specified by MDPs, in practice, there are inevitable biases induced by the sampling methods. The most straight-forward methods generate $\mathcal{P}, \mu_{\mathcal{R}}, \Sigma_{\mathcal{R}}$ using Gaussian and uniform distributions. However, our analysis revealed that tasks generated in this way exhibited simplistic structural patterns. To effectively search “high-quality” MDPs that present meaningful challenges to learners, we designed the procedural generation algorithm based on the following principle:

Under a uniform random policy, the probability of reaching high-valued states is always over 0 but decreases at least exponentially with n_s .

We use a *banded transition kernel* and *composite reward function* to satisfy this constraint, while preserving lower structural bias in the sampling process. Further analyses of the procedural generation are left to Appendix B.1. In subsequent sections, we further demonstrate that AnyMDP tasks achieve the broadest coverage to date across task sets defined within discrete state and action spaces.

Notice that $\mathcal{T}(n_s = 1, n_a)$ represents the widely used multi-armed bandits benchmark for ICRL [6, 15, 20]. As the number of states n_s increases, tasks demand progressively more sophisticated reasoning over delayed rewards

and complex state spaces. This transition evolves the problem from a simple multi-armed bandit framework to a full reinforcement learning paradigm, where long-term planning and environmental interaction become critical. Furthermore, since the ground truth dynamics \mathcal{P} and reward function \mathcal{R} are known within the simulation environment, this setup enables straightforward computation of the oracle solution through value iteration [60].

3.2 Modeling and Training Framework

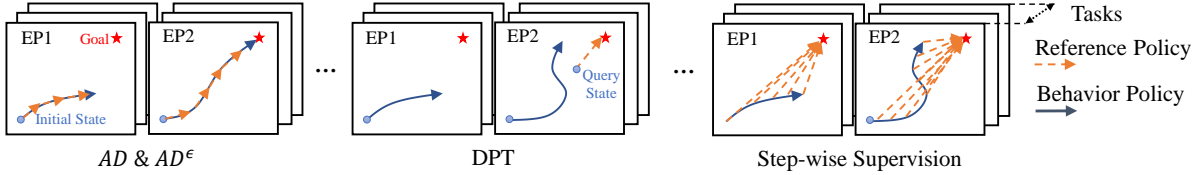


Figure 1: Comparison of the learning pipelines and data formulation of different ICRL methods (AD, AD^ϵ , DPT) and our methods (step-wise supervision, SS), all of which are based on supervised learning.

Step-wise supervision (SS): Meta-training for ICRL using RL or Evolution Strategies faces significant challenges, including cumbersome infrastructure requirements and high computational costs. Recent advances in supervised learning-based meta-training methods—such as Algorithm Distillation (AD) [12], AD^ϵ [14], and Decision Pre-Training Transformers (DPT) [15]—have shown promise for scalable ICRL meta-training. However, a critical challenge arises during inference: contextual trajectories are generated by the model itself, creating an unavoidable gap between training-time and inference-time trajectories. This discrepancy can lead to catastrophic failures during deployment. While leveraging diverse behavior trajectories has been shown to mitigate this issue [15], it introduces a new challenge of maintaining training efficiency. To address these limitations, we propose step-wise supervision (SS), a framework inspired by DPT and data aggregation techniques for imitation learning [61, 62]. Our approach hinges on two key policies: The *behavior policy* refers to the policy executed to generate trajectories during training. The *reference policy* refers to the target policy to be imitated, which remains decoupled from direct execution. Decoupling the behavior and reference policies enables the introduction of diversity into the behavior policy, thereby reducing the discrepancy between training and inference trajectories while maintaining the optimality of the reference policy, as shown in Figure 1. Unlike DPT, which imitates only one-step action conditioned on a trajectory, our step-wise supervision framework is inherently designed to align with high-efficiency chunk-wise training pipelines for sequence models such as Transformers [63] and their optimized variants [64, 65].

Inducing prior knowledge into ICRL: For SS, which employs diverse policies for trajectory generation, prior knowledge becomes crucial for interpreting actions derived from heterogeneous policies [66]. This motivates the incorporation of prior knowledge, specifically metadata indicating the policy used to generate each action. In this work, we implement a diverse set of behavior policies $\Pi = \{\pi^{(b)}\}$, with (b) denoting the behavior policies. $\pi^{(b)}$ comprises seven distinct types, including myopic greedy, oracle, Q-learning, and model-based reinforcement learning, denoted by a marker $tag(\pi) \in \{0, \dots, 6\}$. To handle unseen or unclassified policies, we reserve an additional identifier “Unk” with $m = 7$. The trajectory is denoted by $h_T(\tau, \pi) = [(s_1, g_1, a_1, r_1), \dots, (s_t, g_t, a_t, r_t)]$, where $s_t \in \mathcal{S}$, $a_t \in \mathcal{A}$, $a_t \sim \pi^{(b)}(s_t)$, $r_t \sim \mathcal{R}(s_t, a_t, s_{t+1})$, and $g_t = g(a_t) = tag(\pi^{(b)})$ denotes the prior knowledge for action.

Data synthesis and meta-training: We use π^* to denote the reference policy, which is the oracle policy with $\gamma > 0.99$. It is then used to label a list of the reference actions step-by-step as $l_T(\tau) = [a_1^*, a_2^*, \dots, a_T^*]$ with $a_t^* \sim p_t^* = \pi^*(s_t)$. Notice that for most of the time $a_t \neq a_t^*$. We first collect the training and validation datasets by:

$$\mathcal{D}(\mathcal{T}) = \{ \langle h_T(\tau, \pi), l_T(\tau) \rangle \mid \tau \sim \mathcal{T}, \pi \sim \Pi \} \quad (2)$$

We then meta-train the model in the dataset by optimizing the following target:

$$p_1^\theta, p_2^\theta, \dots, p_t^\theta = \text{Causal}_\theta(s_0, g_0, a_0, r_0, s_1, \dots, s_2, \dots, s_t). \quad (3)$$

$$\text{Minimize} : \mathcal{L} \propto - \sum_{h_T, l_T \in \mathcal{D}} \sum_t w_t \log p_t^\theta(a_t^*) \quad (4)$$

which is also shown in Figure 2.

Scaling up the trajectory length: Extending ICL to complex tasks at scale requires efficient modeling of very long contexts. While the Transformer [63] suffers from both memory limits and computation cost limits for long sequences, we leverage linear attention architectures, such as gated slot attention (GSA) [65] layers and RWKV-7 [67], to extend sequence length scalability, achieving linear computational scaling during inference. To further break down the limitation in context length, we break a long sequence h_T into K segments $[0, T_1], [T_1 + 1, T_2], \dots, [T_{K-1} + 1, T_K]$.

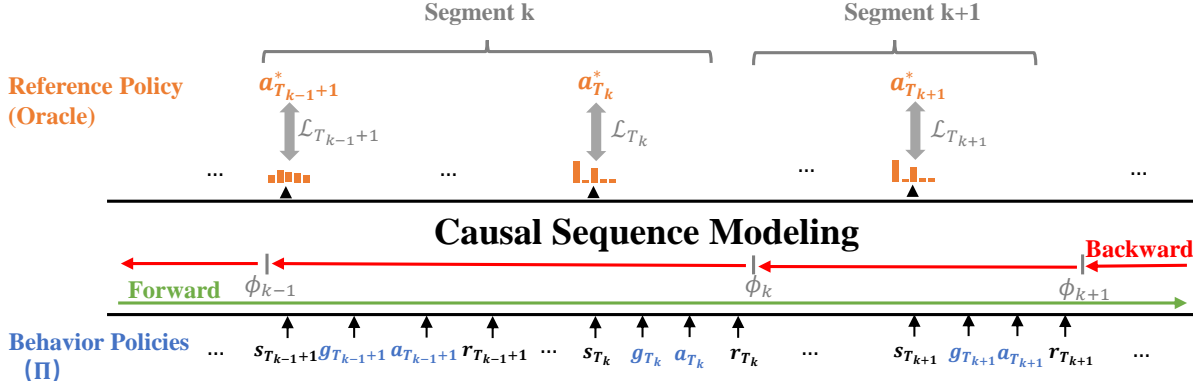


Figure 2: OmniRL model structure and training framework

Table 1: We pick the result achieving its best episode performance within 10,000 episodes for each model, and list the performances, the average steps and episodes required to achieve the score. The hyper-parameters for Q-Learning and PPO are optimized under the evaluated task or task set. The episode performances are normalized to a scale of 0.0 (uniform random policy) to 1.0 (oracle policy). Results for AnyMDP tasks \mathcal{T}_{tst} are averaged over 64 tasks per class, while results for Gymnasium tasks are averaged over 3 independent runs for each task. Notably, all evaluated tasks do not overlap with the OmniRL training task set; furthermore, Gymnasium, DarkRoom, and Bandits tasks are entirely absent from OmniRL’s training regimen.

ENVIRONMENTS	PERFORMANCES / AVG. Steps COST / AVG. Episodes COST		
	TQL-UCB	PPO	OMNIRL(OURS)
$\mathcal{T}_{tst}(1, 5)$ (BANDITS)	92.1%/100/100	95.6%/1.2K/1.2K	82.5%/103/103
$\mathcal{T}_{tst}(16, 5)$	92.0%/297K/4.7K	90.6%/476K/9.7K	95.3%/2.0K/29
$\mathcal{T}_{tst}(32, 5)$	84.7%/616K/5.6K	72.2%/618K/9.7K	90.3%/6.5K/47
$\mathcal{T}_{tst}(64, 5)$	83.7%/1.1M/5.1K	58.3%/1.1M/9.4K	91.3%/7.7K/25
$\mathcal{T}_{tst}(128, 5)$	73.2%/1.8M/6.9K	49.0%/1.3M/8.6K	80.2%/36.3K/100
CLIFFWALKING	100%/3.1K/35	95.9%/99.3K/2.7K	100%/3.0K/65
FROZENLAKE (NON-SLIPPERY)	95.3%/23.6K/3.7K	96.8%/18.2K/2.1K	99.8%/0.3K/35
FROZENLAKE (SLIPPERY)	96%/208K/10.0K	95.6%/73.6K/4.7K	79.5%/7.7K/245
DISCRETE-PENDULUM (G=1)	94.9%/22K/110	99.3%/198K/990	90.5%/8K/40
DISCRETE-PENDULUM (G=5)	99.7%/426K/2.13K	99.8%/132K/660	91.8%/34K/170
DISCRETE-PENDULUM (G=9.8)	90.2%/2.0M/10.0K	98.3%/186K/930	73.4%/33K/165
SWITCH2 (MULTI-AGENT)[68]	98%/3.8K/110	–	80.4%/2.8K/100
DARKROOM (6X6)	98.1%/6.2K/481	97.6%/10.6K/560	95.2%/845/40
DARKROOM (8X8)	96.8%/24.5K/2.0K	96.7%/15.9K/930	93.8%/1.5K/40
DARKROOM (10X10)	89%/31.1K/1.7K	92.3%/15.7K/570	91.7%/2.8K/100

The forward pass is calculated recurrently across the segments, and the backward calculation is performed within each segment. The gradient for the memory states of the linear attention layer ϕ_t is blocked across the segments. Equation (3) is thereby replaced by:

$$p_{T_k+1}^\theta, \dots, p_{T_{k+1}}^\theta, \phi_{k+1} = \text{Causal}_\theta(\text{SG}(\phi_k), s_{T_k+1}, \dots, s_{T_k+2}, \dots, s_{T_{k+1}}) \quad (5)$$

with SG representing stopping gradient. In the meta-training process, the gradients are calculated within each segment and accumulated in cache first. They are applied to the parameters only at the end of the trajectory.

4 Experiments

4.1 Demonstration of Generalization and Scalability

We first validate the representational capability of AnyMDP tasks as universal MDPs. To this end, we collect a dataset $\mathcal{D}_{tra}(\mathcal{T}(n_s, n_a))$ comprising 512K sequences for training, where $n_s \in [16, 128]$, $n_a = 5$. The length of

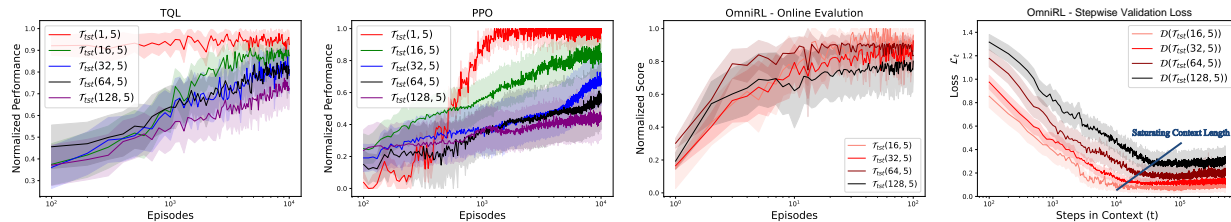


Figure 3: Performance comparison of TQL-UCB, PPO, and OmniRL on test tasks $|\mathcal{T}_{tst}| = 64$. The shaded regions denote 95% confidence intervals. Online evaluation performance is measured across *episodes*. Grid search on the hyperparameters for PPO and TQL-UCB is conducted independently within each task group to achieve their best performance at the final episodes. Additionally, we plot the step-wise validation loss of OmniRL on validation dataset $\mathcal{D}(\mathcal{T}_{tst})$, generated using the same data synthesis methodology as the training dataset but applied to test tasks. The validation loss exhibits strong alignment with online-RL evaluation results.

each sequence T is $12K$, resulting in a total of $6B$ time steps. For testing, we independently sample tasks \mathcal{T}_{tst} with $n_s \in \{1, 16, 32, 64, 128\}$, ensuring each n_s group contains 256 tasks.

The meta-training process is primarily conducted using 8 Nvidia Tesla A800 GPUs. We use a batch size of 5 per GPU, divided into segments (chunks) of 2K steps each. We optimize using the AdamW algorithm with a learning rate that decays from a peak value of 2×10^{-4} . The average time cost per iteration is 8 seconds for trajectories with $T = 12K$, and this cost increases linearly with sequence length. For more details please check Appendix C.2. For the causal sequence model, we evaluate four architectures: RWKV-7 [67], Gated Delta-Net (GDN) [69], Gated Self-Attention (GSA) [65], Mamba2 [70]. In previous tests, model architectures of the Linear Attention type outperformed Transformers in both training efficiency and context memory length. Therefore, the experiments in the figure Figure 4 focus exclusively on linear-attention architectures. The test results are largely consistent with the conclusions in language processing, demonstrating the capability of AnyMDP to serve as a benchmark for long-term sequence modeling. After comparing computational efficiency and performance, we select RWKV-7 for subsequent experiments.

Without any further parameter tuning, we evaluate our model, namely *OmniRL*, on both unseen AnyMDP tasks in Figure 3, Gymnasium tasks, and DarkRoom [12] in Figure 16, and those performances are shown in Table 1. Notably, unlike previous ICRL works, our training set does not include any instances of DarkRoom. In our experiments, the selected tasks are constrained to environments with observation spaces of dimension $n_s \leq 128$ and action spaces of dimension $n_a \leq 5$. For environments with continuous observation spaces, such as *Pendulum-v1*, we manually discretize the observation space into 60 discrete classes using a grid-based discretization method. To adapt OmniRL that is trained with $n_a = 5$ to environments with less actions ($n_a < 5$), we reassign unused actions to valid ones. This further demonstrates the compatibility of OmniRL across environments with varying action space dimensions. We also found that proper reward shaping is important for OmniRL to work, as shown in Figure 14; the details can be found at Appendix C.3.

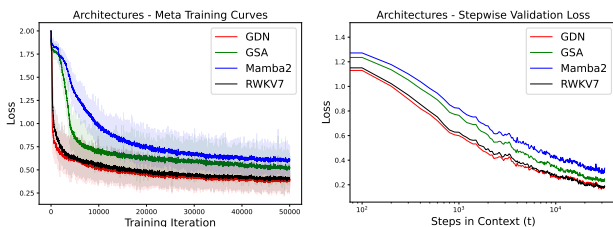


Figure 4: Comparison of meta-training dynamics across AnyMDP dataset of $6B$ time steps and step-wise validation loss for different model architectures.

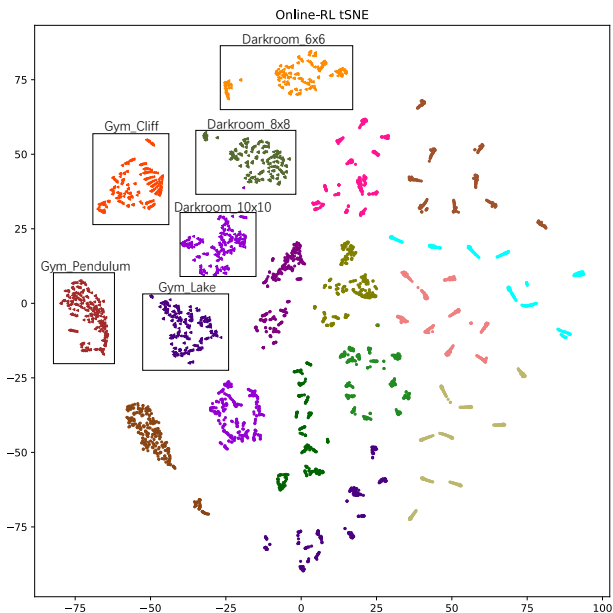


Figure 5: t-SNE visualization of the trajectory of the memory states (ϕ_t) of OmniRL in online-RL evaluation with variant environments. The unboxed points correspond to $\mathcal{T}(16, 5)$. Trajectories originating from the same environment are represented in the same color.

In Table 1, we compare the normalized performance, episode cost, and step costs of OmniRL, classical Tabular Q-learning (TQL) [71] with upper confidence bound (UCB) [72] (TQL-UCB for short), and Proximal Policy Optimization (PPO) [73]. Results show that OmniRL, when meta-trained exclusively on the proposed AnyMDP tasks, effectively adapts to most Gymnasium tasks, validating the representational capability of AnyMDP tasks. This result also demonstrates OmniRL’s superior sample efficiency, which aligns with prior ICRL findings. Notably, despite being trained solely on single-agent tasks, OmniRL adapts to multi-agent tasks like Switch2 by configuring observation spaces, enabling emergent inter-agent cooperation without explicit multi-agent interaction during training and thus decoupling cooperative behavior emergence from centralized mechanisms. Furthermore, in line with expectations, solving AnyMDP tasks becomes more difficult with increased state (n_s) or action (n_a) space size, with PPO proving more sensitive to action space extension and TQL-UCB more vulnerable to state space growth, as illustrated in Figure 9.

Visualizing ICRL. ICRL with linear attention captures all the information required to solve the environment in its memories (ϕ_t). We perform a comprehensive t-SNE analysis to examine how these memories transform across different tasks during Online-RL evaluation. As shown in Figure 5, the clustering patterns confirm the distinct task distributions of Gym, Darkroom, and AnyMDP. Notably, Darkroom and Gym clusters are predominantly located in the top-left region, while AnyMDP occupies a broader spatial area, reflecting its greater diversity. This spatial differentiation emphasizes AnyMDP’s unique characteristics and highlights OmniRL’s strong generalization ability across diverse tasks.

4.2 OmniRL Performs Both Offline and Online Learning Better

For the ablation study and comparison with the other methods including AD, AD^ϵ , and DPT, we collect a smaller dataset with $|\mathcal{D}_{small}|$ comprising 128K sequences for training, where $n_s = 16, n_a = 5, T = 8K$, with a total of 1B time steps. Figure 6 summarizes the performance of different methods trained on \mathcal{D}_{small} with identical training iterations. The comparison includes AD, AD^ϵ , DPT, OmniRL, and OmniRL (w/o a priori) where the prior info g_t is removed from the sequence.

We examine the performance of different methods with different initial contexts: (1) Online-RL: The agent starts with an empty trajectory ($h_0 = \emptyset$). (2) Offline-RL: The agent starts with an existing context derived from imperfect demonstrations (e.g., disturbed oracle policy) ($h_0 = h^\pi$). (3) Imitation Learning: The agent starts with an existing context derived from oracles ($h_0 = h^{(exp)}$). For all three categories, the subsequent interactions are continually added to the context. Therefore, the models differ only in their initial memory or cache. The evaluation assesses the agents’ abilities in two key areas: their capacity to exploit existing information and their ability to explore and exploit continually. In the results in Figure 6, OmniRL and OmniRL (w/o a priori) surpass AD, AD^ϵ , and DPT with large gap, validating the effectiveness of Step-wise Supervision (SS). OmniRL (w/o a priori) lags behind OmniRL with a noticeable gap in all three groups, demonstrating the effectiveness of integrating the prior information. Table 2 and Figure 17 further demonstrate that the offline-learning ability of OmniRL can generalize to Gymnasium environments.

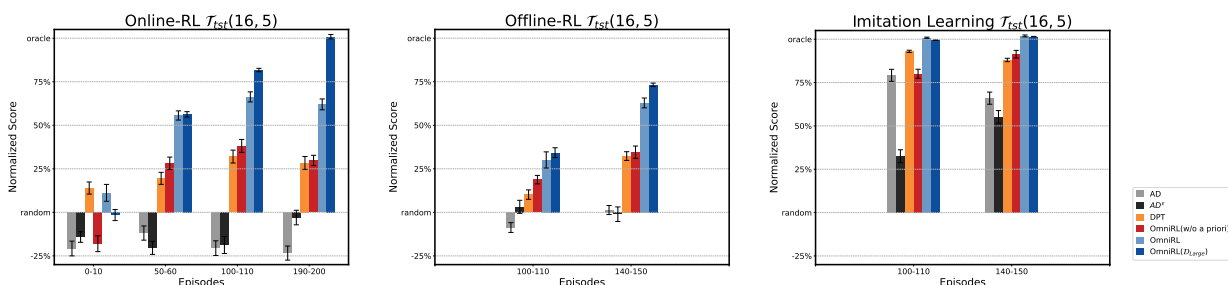


Figure 6: Evaluation results of AD, AD^ϵ , DPT, and OmniRL on 32 AnyMDP tasks, with 3 groups of initial demonstrations to assess the capabilities of online-RL, offline-RL, and imitation learning. For offline-RL and imitation learning, the agent is initialized with the context including 100 episodes of demonstration. The results demonstrate the effectiveness of Step-wise Supervision (SS) and the integration of prior information.

4.3 Emergence of General-Purpose ICRL by Increasing Task Number

We validate task diversity’s critical role in ICRL via independent meta-training across four datasets, each $\mathcal{D}(\mathcal{T}_{tra}(16, 5))$ containing 128K sequences but differing in task numbers ($|\mathcal{T}_{tra}| \in \{100, 1K, 10K, 128K\}$). Note that different trajectories can be generated from a single task, arising from the diverse behavior policies and random sampling in

Table 2: We select four Gymnasium environments to evaluate the performance of Offline RL and Imitation Learning. In each environment, both oracle and random teacher demonstrations are provided. Conservative Q-Learning (CQL) [74] updates its value table using the demonstration data, while OmniRL loads the data in its memory. The performance across the first 0–20 episodes reflects the effectiveness of Offline RL and Imitation Learning, whereas the performance in episodes 180–200 demonstrates the outcomes after online learning.

ENVIRONMENTS	TEACHER(PERFORMANCE)	0~20/180~200 EPISODES PERFORMANCE	
		CQL	OMNIRL
FROZENLAKE (SLIPPERY)	ORACLE (77.80%)	76.61% / 76.11%	70.12% / 77.27%
	RANDOM (1.46%)	37.79% / 72.36%	54.3% / 67.38%
CLIFF	ORACLE (-13)	-30.8 / -13	-13 / -13
	RANDOM (-109.84)	-560.2 / -16.2	-91 / -17
DISCRETE-PENDULUM (G=5)	ORACLE (-153.81)	-605.89 / -258.22	-180 / -127
	RANDOM (-941.65)	-1062.40 / -184.29	-646 / -208
DARKROOM (10X10)	ORACLE (0.22)	0.23 / 0.22	0.22 / 0.21
	RANDOM (-15.07)	-4.05 / 0.21	0.09 / 0.19

both decision and transition. We examine how the validation losses \mathcal{L}_t on both seen and unseen tasks change with the number of meta-training iterations (outer-loop steps) and steps in context t (inner-loop steps) simultaneously; the results are shown in Figure 7. We remark the following observations:

Task number is crucial to the generalization of ICRL. The previous investigation on ICL [26, 29] emphasizes the importance of “burstiness”. Our results demonstrate for the first time that even when using “bursty” sequences alone, both the number of tasks and their overall diversity remain critically important. Specifically, in groups with $|\mathcal{T}_{\text{train}}| \leq 10K$, over-training leads to a transiency of ICL [19] in unseen tasks but a continued improvement in seen tasks. These findings confirm and extend the discovery of the “task identification” phase mentioned in Kirsch et al. [32], Pan et al. [75]. Drawing on the theories of ICL and IWL in Chan et al. [31], a possible explanation is that IWL dominates performance, with the model memorizing tasks and ICL selecting the correct one, leading to fast seen-task adaptation but poor unseen generalization. As the number of tasks increases continuously, the model becomes more dependent on ICL since memorizing task-specific information becomes less feasible. This is characterized by the improved generalization to unseen tasks and longer adaptation periods in both seen and unseen tasks, as shown in Figure 7.

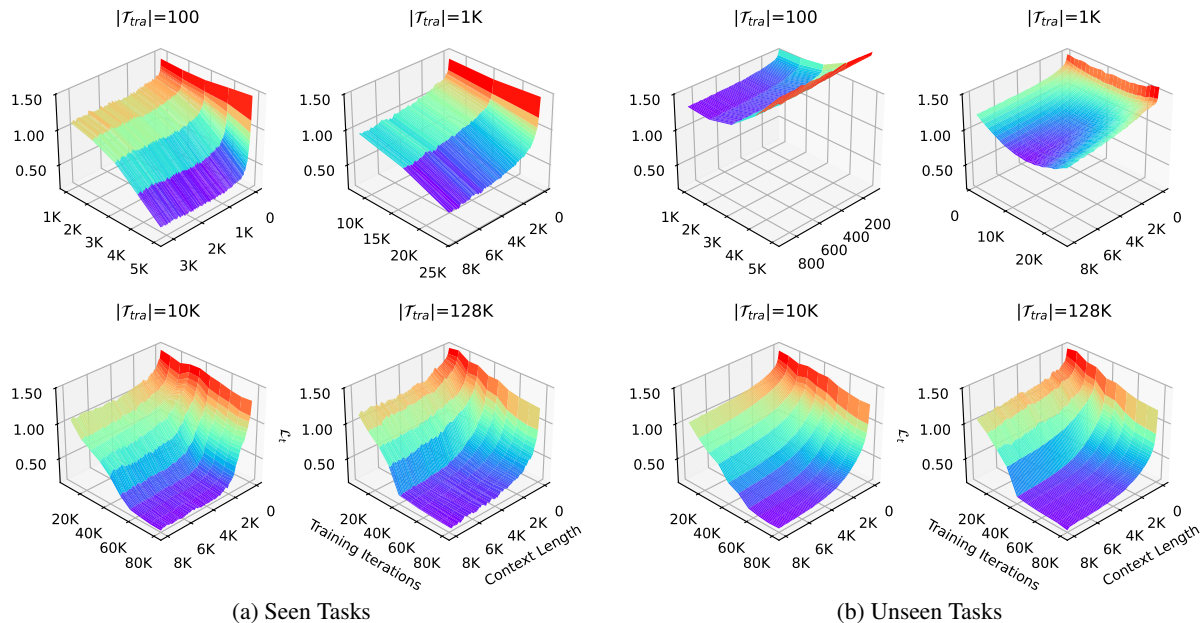
Generalization of ICRL can be at odds with its zero-shot or few-shot performance. Our results highlight a key insight on ICRL evaluation. Most previous ICRL works assess performance based on the average results over a fixed, short context span. However, our findings indicate that more generalized in-context learners may actually perform worse in zero-shot and even few-shot evaluations, particularly when there is significant overlap between the training and evaluation sets, i.e., when evaluation sets are closer to seen tasks. Therefore, we argue that it is more critical to focus on the *asymptotic performance* of a learner. This can be effectively evaluated by examining the performance at the final steps or episodes of a sufficiently long context, rather than short-term metrics.

5 Conclusions and Discussions

We propose a scalable, low-structural-bias task set for benchmarking and investigating Inverse Contextual Reinforcement Learning (ICRL). Our framework introduces two key innovations: stepwise supervision and prior information induction, creating a more efficient ICRL system. Experimental results demonstrate that our model achieves superior generalization across RL tasks compared to existing approaches. The proposed model generalizes to a broader range of RL tasks than ever before. Our work introduces a more scalable testbed for ICRL research.

Broader impact: Complementing prior studies, our findings highlight that task diversity and sequence length—alongside sequence burstiness—are key determinants of general ICRL. Our results also advocate shifting evaluation metrics toward asymptotic performance measures. This work further motivates the construction of carefully curated synthetic datasets specifically designed for large-scale meta-training.

Limitations and future work: We acknowledge that the discrete state and action space is the most significant limitation of this work, as it restricts its application to environments with continuous state and action spaces. Extending this work to continuous and partially observable environments, as well as incorporating additional modalities, would significantly broaden its scope of application.



Validation set	Metrics	$ \mathcal{T}_{tra} $			
		100	1K	10K	128K
Seen tasks	$\max(d_t)$	> 81.0%	> 65.4%	$\geq 86.6\%$	$\geq 84.5\%$
	$\min(t)$ s.t. $d_t \geq 80\%$	0.88K	-	2.4K	5.2K
Unseen tasks	$\max(d_t)$	17.9%	38.0%	84.4%	$\geq 84.8\%$
	$\min(t)$ s.t. $d_t \geq 80\%$	-	-	3.9K	5.1K
	$\max(d_t)$ achieved at iteration	2K	14K	72K	$\geq 80K$

Figure 7: Position-wise validation losses (\mathcal{L}_t , where lower values indicate better performance) and their properties on both seen and unseen tasks across meta-training iterations, varying context lengths, and variant number of tasks $|\mathcal{T}_{tra}|$. Each of the 4 groups of training data had 128K sequences, which were generated from 100, 1K, 10K, and 128K tasks, respectively. Each dataset underwent meta-training for up to 80K iterations. In the table, the notation “>” indicates values that could not be fully determined due to training being stopped early when performance on unseen tasks began to deteriorate. The normalized gain of ICL is defined as $d_t = 1 - \mathcal{L}_t / \mathcal{L}_0$, representing the improvement of performance as the context (t) increases. The table summarizes key findings of this study: as the number of tasks increases, the minimum step cost required to achieve an 80% normalized gain of ICL also increases.

References

- [1] A. Radford, J. W. Kim, C. Hallacy, A. Ramesh, G. Goh, S. Agarwal, G. Sastry, A. Askell, P. Mishkin, J. Clark, et al., Learning transferable visual models from natural language supervision, in: International conference on machine learning, PMLR, 2021, pp. 8748–8763.
- [2] D. Driess, F. Xia, M. S. Sajjadi, C. Lynch, A. Chowdhery, B. Ichter, A. Wahid, J. Tompson, Q. Vuong, T. Yu, et al., Palm-e: An embodied multimodal language model, arXiv preprint arXiv:2303.03378 (2023).
- [3] H. Touvron, T. Lavril, G. Izacard, X. Martinet, M.-A. Lachaux, T. Lacroix, B. Rozière, N. Goyal, E. Hambro, F. Azhar, et al., Llama: Open and efficient foundation language models, arXiv preprint arXiv:2302.13971 (2023).
- [4] J. Achiam, S. Adler, S. Agarwal, L. Ahmad, I. Akkaya, F. L. Aleman, D. Almeida, J. Altschmidt, S. Altman, S. Anadkat, et al., Gpt-4 technical report, arXiv preprint arXiv:2303.08774 (2023).
- [5] T. Brown, B. Mann, N. Ryder, M. Subbiah, J. D. Kaplan, P. Dhariwal, A. Neelakantan, P. Shyam, G. Sastry, A. Askell, et al., Language models are few-shot learners, Advances in neural information processing systems 33 (2020) 1877–1901.
- [6] Y. Duan, J. Schulman, X. Chen, P. L. Bartlett, I. Sutskever, P. Abbeel, RL²: Fast reinforcement learning via slow reinforcement learning, arXiv preprint arXiv:1611.02779 (2016).

- [7] A. Santoro, S. Bartunov, M. Botvinick, D. Wierstra, T. Lillicrap, Meta-learning with memory-augmented neural networks, in: International conference on machine learning, PMLR, 2016, pp. 1842–1850.
- [8] S. Garg, D. Tsipras, P. S. Liang, G. Valiant, What can transformers learn in-context? a case study of simple function classes, *Advances in Neural Information Processing Systems* 35 (2022) 30583–30598.
- [9] S. Reed, K. Zolna, E. Parisotto, S. G. Colmenarejo, A. Novikov, G. Barth-marion, M. Giménez, Y. Sulsky, J. Kay, J. T. Springenberg, et al., A generalist agent, *Transactions on Machine Learning Research* (2022).
- [10] L. Fu, H. Huang, G. Datta, L. Y. Chen, W. C.-H. Panitch, F. Liu, H. Li, K. Goldberg, In-context imitation learning via next-token prediction, in: 1st Workshop on X-Embodiment Robot Learning, 2024.
- [11] V. Vosylius, E. Johns, Few-shot in-context imitation learning via implicit graph alignment, in: 7th Annual Conference on Robot Learning, 2024.
- [12] M. Laskin, L. Wang, J. Oh, E. Parisotto, S. Spencer, R. Steigerwald, D. Strouse, S. S. Hansen, A. Filos, E. Brooks, et al., In-context reinforcement learning with algorithm distillation, in: *NeurIPS 2022 Foundation Models for Decision Making Workshop*, 2022.
- [13] J. Grigsby, L. Fan, Y. Zhu, Amago: Scalable in-context reinforcement learning for adaptive agents, in: *The Twelfth International Conference on Learning Representations*, 2024.
- [14] I. Zisman, V. Kurenkov, A. Nikulin, V. Sini, S. Kolesnikov, Emergence of in-context reinforcement learning from noise distillation, in: *Forty-first International Conference on Machine Learning*, 2024.
- [15] J. Lee, A. Xie, A. Pacchiano, Y. Chandak, C. Finn, O. Nachum, E. Brunskill, Supervised pretraining can learn in-context reinforcement learning, *Advances in Neural Information Processing Systems* 36 (2024).
- [16] S. Dohare, J. F. Hernandez-Garcia, Q. Lan, P. Rahman, A. R. Mahmood, R. S. Sutton, Loss of plasticity in deep continual learning, *Nature* 632 (2024) 768–774.
- [17] G. Lior, Y. Shalev, G. Stanovsky, A. Goldstein, Computation or weight adaptation? rethinking the role of plasticity in learning, *bioRxiv* (2024) 2024–03.
- [18] J. Wei, Y. Tay, R. Bommasani, C. Raffel, B. Zoph, S. Borgeaud, D. Yogatama, M. Bosma, D. Zhou, D. Metzler, et al., Emergent abilities of large language models, *Transactions on Machine Learning Research* (2022).
- [19] A. Singh, S. Chan, T. Moskowitz, E. Grant, A. Saxe, F. Hill, The transient nature of emergent in-context learning in transformers, *Advances in Neural Information Processing Systems* 36 (2024).
- [20] N. Mishra, M. Rohaninejad, X. Chen, P. Abbeel, A simple neural attentive meta-learner, in: *International Conference on Learning Representations*, 2018.
- [21] S. Thrun, L. Pratt, Learning to learn: Introduction and overview, in: *Learning to learn*, Springer, 1998, pp. 3–17.
- [22] C. Finn, P. Abbeel, S. Levine, Model-agnostic meta-learning for fast adaptation of deep networks, in: *International conference on machine learning*, PMLR, 2017, pp. 1126–1135.
- [23] D. L. Barabási, A. Ferreira Castro, F. Engert, Three systems of circuit formation: assembly, updating and tuning, *Nature Reviews Neuroscience* (2025) 1–12.
- [24] Y. Chen, R. Zhong, S. Zha, G. Karypis, H. He, Meta-learning via language model in-context tuning, *arXiv preprint arXiv:2110.07814* (2021).
- [25] J. Coda-Forno, M. Binz, Z. Akata, M. Botvinick, J. Wang, E. Schulz, Meta-in-context learning in large language models, *Advances in Neural Information Processing Systems* 36 (2023) 65189–65201.
- [26] S. C. Raparthy, E. Hambro, R. Kirk, M. Henaff, R. Raileanu, Generalization to new sequential decision making tasks with in-context learning, in: *Proceedings of the 41st International Conference on Machine Learning*, 2024, pp. 42138–42158.
- [27] E. Edelman, N. Tsilivis, B. Edelman, E. Malach, S. Goel, The evolution of statistical induction heads: In-context learning markov chains, *Advances in Neural Information Processing Systems* 37 (2024) 64273–64311.

- [28] T. J. Liu, N. Boulle, R. Sarfati, C. Earls, Llms learn governing principles of dynamical systems, revealing an in-context neural scaling law, in: Proceedings of the 2024 Conference on Empirical Methods in Natural Language Processing, Association for Computational Linguistics, Miami, Florida, USA, 2024, pp. 15097–15117.
- [29] S. Chan, A. Santoro, A. Lampinen, J. Wang, A. Singh, P. Richemond, J. McClelland, F. Hill, Data distributional properties drive emergent in-context learning in transformers, *Advances in Neural Information Processing Systems* 35 (2022) 18878–18891.
- [30] Y. Zhao, Y. Qu, K. Staniszewski, S. Tworkowski, W. Liu, P. Miłoś, Y. Wu, P. Minervini, Analysing the impact of sequence composition on language model pre-training, in: Proceedings of the 62nd Annual Meeting of the Association for Computational Linguistics (Volume 1: Long Papers), 2024, pp. 7897–7912.
- [31] B. Chan, X. Chen, A. György, D. Schuurmans, Toward understanding in-context vs. in-weight learning, in: The Thirteenth International Conference on Learning Representations, 2025.
- [32] L. Kirsch, J. Harrison, J. Sohl-Dickstein, L. Metz, General-purpose in-context learning by meta-learning transformers, *arXiv preprint arXiv:2212.04458* (2022).
- [33] N. Wies, Y. Levine, A. Shashua, The learnability of in-context learning, *Advances in Neural Information Processing Systems* 36 (2024).
- [34] S. C. Chan, I. Dasgupta, J. Kim, D. Kumaran, A. K. Lampinen, F. Hill, Transformers generalize differently from information stored in context vs in weights, *arXiv preprint arXiv:2210.05675* (2022).
- [35] J. Von Oswald, E. Niklasson, E. Randazzo, J. Sacramento, A. Mordvintsev, A. Zhmoginov, M. Vladymyrov, Transformers learn in-context by gradient descent, in: International Conference on Machine Learning, PMLR, 2023, pp. 35151–35174.
- [36] S. M. Xie, A. Raghunathan, P. Liang, T. Ma, An explanation of in-context learning as implicit bayesian inference, in: International Conference on Learning Representations, 2022.
- [37] L. Kirsch, J. Harrison, D. Freeman, J. Sohl-Dickstein, J. Schmidhuber, Towards general-purpose in-context learning agents, *Workshop on Distribution Shifts, 37th Conference on Neural Information ...*, 2023.
- [38] F. Wang, C. Lin, Y. Cao, Y. Kang, Benchmarking general purpose in-context learning, *arXiv preprint arXiv:2405.17234* (2024).
- [39] E. Najarro, S. Risi, Meta-learning through hebbian plasticity in random networks, *Advances in Neural Information Processing Systems* 33 (2020) 20719–20731.
- [40] F. Wang, H. Tian, H. Xiong, H. Wu, J. Fu, Y. Cao, Y. Kang, H. Wang, Evolving decomposed plasticity rules for information-bottlenecked meta-learning, *Transactions on Machine Learning Research* (2022).
- [41] M. G. Azar, I. Osband, R. Munos, Minimax regret bounds for reinforcement learning, in: International conference on machine learning, PMLR, 2017, pp. 263–272.
- [42] T. Xu, Z. Li, Y. Yu, Error bounds of imitating policies and environments, *Advances in Neural Information Processing Systems* 33 (2020) 15737–15749.
- [43] Z. Zhang, A. Liniger, D. Dai, F. Yu, L. Van Gool, End-to-end urban driving by imitating a reinforcement learning coach, in: Proceedings of the IEEE/CVF international conference on computer vision, 2021, pp. 15222–15232.
- [44] A. Raventós, M. Paul, F. Chen, et al., Pretraining task diversity and the emergence of non-bayesian in-context learning for regression, in: *Advances in Neural Information Processing Systems*, volume 36, 2023, pp. 14228–14246.
- [45] O. E. L. Team, A. Stooke, A. Mahajan, C. Barros, C. Deck, J. Bauer, J. Sygnowski, M. Trebacz, M. Jaderberg, M. Mathieu, et al., Open-ended learning leads to generally capable agents, *arXiv preprint arXiv:2107.12808* (2021).
- [46] C. G. I. Team, A. Bhoopchand, B. Brownfield, A. Collister, A. D. Lago, A. Edwards, R. Everett, A. Frechette, Y. G. Oliveira, E. Hughes, et al., Learning robust real-time cultural transmission without human data, *arXiv preprint arXiv:2203.00715* (2022).

- [47] J. Bauer, K. Baumli, F. Behbahani, A. Bhoopchand, N. Bradley-Schmieg, M. Chang, N. Clay, A. Collister, V. Dasagi, L. Gonzalez, et al., Human-timescale adaptation in an open-ended task space, in: Proceedings of the 40th International Conference on Machine Learning, 2023, pp. 1887–1935.
- [48] Q. Wang, Y. Wang, Y. Wang, et al., Can in-context learning really generalize to out-of-distribution tasks?, 2024. ArXiv preprint arXiv:2410.09695.
- [49] X. B. Peng, M. Andrychowicz, W. Zaremba, P. Abbeel, Sim-to-real transfer of robotic control with dynamics randomization, in: 2018 IEEE international conference on robotics and automation (ICRA), IEEE, 2018, pp. 3803–3810.
- [50] T. Yu, D. Quillen, Z. He, R. Julian, K. Hausman, C. Finn, S. Levine, Meta-world: A benchmark and evaluation for multi-task and meta reinforcement learning, in: Conference on robot learning, PMLR, 2020, pp. 1094–1100.
- [51] L. N. Alegre, F. Felten, E.-G. Talbi, G. Danoy, A. Nowé, A. L. Bazzan, B. C. da Silva, Mo-gym: A library of multi-objective reinforcement learning environments, in: Proceedings of the 34th Benelux Conference on Artificial Intelligence BNAIC/Benelearn, volume 2022, 2022, p. 2.
- [52] K. Cobbe, C. Hesse, J. Hilton, J. Schulman, Leveraging procedural generation to benchmark reinforcement learning, in: International conference on machine learning, PMLR, 2020, pp. 2048–2056.
- [53] J. W. Pedersen, S. Risi, Evolving and merging hebbian learning rules: increasing generalization by decreasing the number of rules, in: Proceedings of the Genetic and Evolutionary Computation Conference, 2021, pp. 892–900.
- [54] A. Nikulin, V. Kurenkov, I. Zisman, A. Agarkov, V. Sinii, S. Kolesnikov, Xland-minigrid: Scalable meta-reinforcement learning environments in jax, arXiv preprint arXiv:2312.12044 (2023).
- [55] S. Morad, R. Kortvelesy, M. Bettini, S. Liwicki, A. Prorok, Popgym: Benchmarking partially observable reinforcement learning, arXiv preprint arXiv:2303.01859 (2023).
- [56] V. Sinii, A. Nikulin, V. Kurenkov, I. Zisman, S. Kolesnikov, In-context reinforcement learning for variable action spaces, in: Proceedings of the 41st International Conference on Machine Learning, 2024, pp. 45773–45793.
- [57] I. Akkaya, M. Andrychowicz, M. Chociej, M. Litwin, B. McGrew, A. Petron, A. Paino, M. Plappert, G. Powell, R. Ribas, et al., Solving rubik’s cube with a robot hand, arXiv preprint arXiv:1910.07113 (2019).
- [58] A. Nikulin, V. Kurenkov, I. Zisman, A. Agarkov, V. Sinii, S. Kolesnikov, Xland-minigrid: Scalable meta-reinforcement learning environments in jax, Advances in Neural Information Processing Systems 37 (2024) 43809–43835.
- [59] E. Akyürek, B. Wang, Y. Kim, J. Andreas, In-context language learning: Architectures and algorithms, in: International Conference on Machine Learning, PMLR, 2024, pp. 787–812.
- [60] R. Bellman, Dynamic programming, Chapter IX, Princeton University Press, Princeton, New Jersey (1958).
- [61] S. Ross, D. Bagnell, Efficient reductions for imitation learning, in: Proceedings of the thirteenth international conference on artificial intelligence and statistics, JMLR Workshop and Conference Proceedings, 2010, pp. 661–668.
- [62] S. Ross, G. Gordon, D. Bagnell, A reduction of imitation learning and structured prediction to no-regret online learning, in: Proceedings of the fourteenth international conference on artificial intelligence and statistics, JMLR Workshop and Conference Proceedings, 2011, pp. 627–635.
- [63] A. Vaswani, Attention is all you need, Advances in Neural Information Processing Systems (2017).
- [64] Y. Li, M. E. Ildiz, D. Papailiopoulos, S. Oymak, Transformers as algorithms: Generalization and stability in in-context learning, in: International Conference on Machine Learning, PMLR, 2023, pp. 19565–19594.
- [65] Y. Zhang, S. Yang, R.-J. Zhu, Y. Zhang, L. Cui, Y. Wang, B. Wang, F. Shi, B. Wang, W. Bi, et al., Gated slot attention for efficient linear-time sequence modeling, in: The Thirty-eighth Annual Conference on Neural Information Processing Systems, 2024.
- [66] L. Chen, K. Lu, A. Rajeswaran, K. Lee, A. Grover, M. Laskin, P. Abbeel, A. Srinivas, I. Mordatch, Decision transformer: Reinforcement learning via sequence modeling, Advances in neural information processing systems 34 (2021) 15084–15097.

- [67] B. Peng, R. Zhang, D. Goldstein, E. Alcaide, H. Hou, J. Lu, W. Merrill, G. Song, K. Tan, S. Utpala, et al., "Rwkv-7" goose" with expressive dynamic state evolution, arXiv preprint arXiv:2503.14456 (2025).
- [68] A. Koul, ma-gym: Collection of multi-agent environments based on openai gym., <https://github.com/koulanurag/ma-gym>, 2019.
- [69] S. Yang, J. Kautz, A. Hatamizadeh, Gated delta networks: Improving mamba2 with delta rule (2025).
- [70] T. Dao, A. Gu, Transformers are ssms: generalized models and efficient algorithms through structured state space duality, in: Proceedings of the 41st International Conference on Machine Learning, 2024, pp. 10041–10071.
- [71] R. S. Sutton, A. G. Barto, et al., Reinforcement learning: An introduction, volume 1, MIT press Cambridge, 1998.
- [72] C. Jin, Z. Allen-Zhu, S. Bubeck, M. I. Jordan, Is q-learning provably efficient?, Advances in neural information processing systems 31 (2018).
- [73] J. Schulman, F. Wolski, P. Dhariwal, A. Radford, O. Klimov, Proximal policy optimization algorithms, arXiv preprint arXiv:1707.06347 (2017).
- [74] A. Kumar, A. Zhou, G. Tucker, S. Levine, Conservative q-learning for offline reinforcement learning, Advances in neural information processing systems 33 (2020) 1179–1191.
- [75] J. Pan, T. Gao, H. Chen, D. Chen, "What in-context learning" learns" in-context: Disentangling task recognition and task learning, in: The 61st Annual Meeting Of The Association For Computational Linguistics, 2023.
- [76] D. Guo, D. Yang, H. Zhang, J. Song, R. Zhang, R. Xu, Q. Zhu, S. Ma, P. Wang, X. Bi, et al., Deepseek-r1: Incentivizing reasoning capability in llms via reinforcement learning, arXiv preprint arXiv:2501.12948 (2025).
- [77] P. C. Wason, J. S. B. Evans, Dual processes in reasoning?, Cognition 3 (1974) 141–154.
- [78] D. Kahneman, Thinking, fast and slow, Farrar, Straus and Giroux (2011).

A Notations

B Details of AnyMDP Environments

B.1 Procedural generation of high-quality MDPs

To effectively sample the tuple $\langle \mathcal{S}, \mathcal{A}, \mathcal{P}, \mathcal{R}, \mathcal{S}_0, \mathcal{S}_E, T_E, \gamma \rangle$ and ensure broad coverage of the task space while providing sufficient challenges for resolution, we propose a procedural generation pipeline, which is detailed in Algorithm 1. This approach is guided by the general principle that states which are more difficult to reach tend to offer greater rewards. The procedural generation methods emphasize two key features: a **banded transition kernel** and a **composite reward function**.

Banded transition kernel: We first demonstrate that this sampling method ensures the reachability of all states while simultaneously guaranteeing that the probability of finding a solution through random exploration decreases at least exponentially.

We focus on the Markov chain (MC) defined by running a uniform random policy on the MDP, where actions are chosen by: $a \sim \pi^\tau(a|s) = \frac{1}{|\mathcal{A}|}$. This Markov chain can be formally represented as $\langle \hat{\mathcal{P}}_\tau, \mathcal{S}_0, \mathcal{S}_E \rangle$, with $\hat{\mathcal{P}}_\tau$ representing the state-state transition kernel as follows:

$$\hat{\mathcal{P}}_\tau(s'|s) = \mathbb{E}_{a \sim \pi^\tau(a|s)} \mathcal{P}(s'|s, a) = P_{\tau, s, s'} \quad (6)$$

We further define the stationary distribution (SD) of the Markov chain P_τ as follows:

$$p_\tau P_\tau = p_\tau \quad (7)$$

Here $p_\tau \in \mathbb{R}^{n_s}$ is a probability vector that sums to 1, representing the asymptotic distribution over the state space under the transition matrix P_τ . With this foundation, we can prove the following:

Table 3: Default simplifications and notations used throughout the paper.

ICL	IN-CONTEXT LEARNING
IWL	IN-WEIGHT LEARNING
ICRL	IN-CONTEXT REINFORCEMENT LEARNING
MC	MARKOV CHAIN
MDP	MARKOV DECISION PROCESS
SS	STEP-WISE SUPERVISION
SD	STATIONARY DISTRIBUTION
<hr/>	
\mathcal{S}	STATE OR OBSERVATION SPACE
\mathcal{S}_0	STATES FOR RESET
\mathcal{S}_E	STATES TRIGGERING TERMINATION
T_E	MAXIMUM LENGTH OF AN EPISODE
$\mathcal{P}(s, a, s')$	TRANSITION FUNCTION OF $s, a \rightarrow s'$
$\mathcal{R}(s, a, s')$	REWARD FUNCTION OF $s, a \rightarrow s'$
γ	DISCOUNT FACTOR FOR REWARDS
\mathcal{A}	ACTION SPACE
Π	A SET / COLLECTION OF POLICIES
$s \in \mathcal{S}$	STATE OR OBSERVATION
$a \in \mathcal{A}$	ACTION
$r \in \mathbb{R}$	REWARD OR FEEDBACK
g	PRIOR INFORMATION OF ACTION
$\pi \in \Pi$	POLICY FUNCTION
$Q^\pi(s, a)$	STATE-ACTION VALUE FUNCTION
$V^\pi(s, a)$	STATE VALUE FUNCTION, $V^\pi(s) = \mathbb{E}_{a \sim \pi}[Q^\pi(s, a)]$
π^*	ORACLE POLICY ACHIEVING HIGHEST EXPECTED EPISODIC REWARDS
$a^* \sim \pi^*$	ACTION GENERATED BY ORACLE POLICY
Q^*, V^*	VALUE FUNCTION WITH ORACLE POLICY
$\tau(n_s, n_a)$	TASK WITH n_s DISCRETE STATES AND n_a DISCRETE ACTIONS
$\mathcal{T}(n_s, n_a)$	A COLLECTION OF TASKS $\tau(n_s, n_a)$
$\mathcal{D}(\mathcal{T})$	DATASET RECORDED FROM EXECUTION ON \mathcal{T}
h_t	A TRAJECTORY $[(s_1, g_1, a_1, r_1), \dots, (s_t, g_t, a_t, r_t)]$
l_t	STEP-WISE SUPERVISION LABELS FOR TRAJECTORY h_t
$p_\tau(s)$	STATIONARY DISTRIBUTION (SD) OF MDP WITH THE POLICY π^τ
θ	PARAMETERS OF A MODEL, KEPT UNCHANGED IN THE INNER LOOP (ICL)
ϕ	CACHES OR MEMORIES, STARTS FROM SCRATCH IN THE INNER LOOP
\mathfrak{o}	AGENT WITH ORACLE POLICY π^*
\mathfrak{q}	Q-LEARNING AGENT
\mathfrak{r}	AGENT WITH RANDOM POLICY
\mathfrak{m}	MODEL-BASED REINFORCEMENT LEARNING AGENT
\mathfrak{o}^ε	AGENT \mathfrak{o} DISTURBED WITH A DECAYING NOISE ε

Theorem 1. For $j > b$, where $b = \max(b_-, b_0) + b_+$, there exists a value $0 < \delta < 1/(b_+ + 1)$. If $\eta > 1 - \delta$, the sampling algorithm described in Algorithm 1 ensures that the random policy Markov chain has a stationary distribution (SD). Specifically, for the state s_j , the SD $p_\tau(s_j)$ satisfies the following bounds:

$$C_1 \varepsilon^{j-b} < p_\tau(s_j) < C_2 (1 - \delta)^{j-b},$$

where C_1 and C_2 are positive constants.

Proof. We began by establishing the upper bound for $p^\tau(s_j)$. Notably, if $\mathcal{S}_E \neq \emptyset$ the upper bound would be further reduced for indices $j > b$, as system termination resets states to indices $j < b_0$. Consequently, it suffices to analyze the case where $\mathcal{S}_E = \emptyset$ as non-empty \mathcal{S}_E only tightens the bound.

Under the conditions that $\sum_{j < i} \hat{\mathcal{P}}(s_j | s_i) > \eta$ if $i > b_-$ and $\forall j > i + b_+$, $\hat{\mathcal{P}}(s_j | s_i) = 0$, we construct a **worst case transition kernel**. This kernel is defined as follows:

$$\forall s_i \text{ with } n_s - b_+ > i > b, \mathcal{P}_+(s_{i-1}) \equiv \eta, \mathcal{P}_+(s_{i+b_+} | s_i) \equiv 1 - \eta, \mathcal{P}_+(\cdot | s_i) \equiv 0 \text{ for other cases.}$$

It follows directly from this construction that $p_\tau(s_j) < p_+(s_j)$ for $j > b$, as \mathcal{P}_+ maximizes transition probabilities to later states under the given constraints.

Algorithm 1 AnyMDP *TaskSampler*

```

1: Input:  $n_s, n_a$  Returns:  $\tau(n_s, n_a)$ 
2: randomly generate: an ordered list arranged from low-valued to high-valued states  $S = [s_1, s_2, \dots, s_{n_s}]$  by
   permute  $\mathcal{S} = \{1, \dots, n_s\}$ 
3: randomly sample: states for reset  $\mathcal{S}_0 \subset \{s_0, s_1, \dots, s_{b_0}\}$ 
4: randomly sample: states triggering termination  $\mathcal{S}_E \subset \mathcal{S}/\mathcal{S}_0$ 
5: for  $i \leftarrow 1$  to  $n_s$  do
6:   randomly sample:  $\hat{\mathcal{P}}_\tau(\cdot|s_i)$ , s.t.
7:      $\forall j > i + b_+$  and  $\forall j < i - b_-$ ,  $\hat{\mathcal{P}}_\tau(s_j|s_i) = 0$  and
8:      $\sum_{j < i} \hat{\mathcal{P}}_\tau(s_j|s_i) > \eta$  if  $i > b_-$  and
9:      $\sum_{j \leq i} \hat{\mathcal{P}}_\tau(s_{i+1}|s_j) > \epsilon$  if  $i < n_s - 1$ 
10:  randomly sample:  $w(s_i, a_k) \forall k \in [1, n_a]$ 
11:  set:  $\mathcal{P}(s_j|s_i, a_k) = \hat{\mathcal{P}}_\tau(s_j|s_i) \exp w(s, a_k) / \sum_a \exp(w(s, a)) \forall j, k$ 
12: end for
13: randomly sample: state-action dependent rewards  $r_{sa} \in \mathbb{R}^{n_s \times n_a}$ 
14: randomly sample: potential  $v_s \in \mathbb{R}^{n_s}$ 
15: repeat
16:  randomly sample: state-wise reward function  $r_s \in \mathbb{R}^{n_s}$ , s.t.  $\forall j > i, r_s(s_j) \geq r_s(s_i)$ 
17:  set:  $\mu_{\mathcal{R}}(s, a, s') = r_{sa}(s, a) + r_s(s') + v_s(s) - v_s(s')$ 
18:  calculate: value function  $V^*(s)$  based on  $\mathcal{P}, \mathcal{R}, \mathcal{S}_0, \mathcal{S}_E$ 
19: until  $V^*(s_g) > \max_{s \in \mathcal{S}_0} V^*(s) + b_V$ 
20: final validate: calculate oracle policy steady state distribution ( $p_o$ )
21:   if  $-\sum_s p_o \log p_o / \log n_s > H_0$  then accept, else resample the task.

```

By the definition of the SD, we have:

$$\eta p_{i,i-1} + (1 - \eta) p_{i,i+b_+} = p_{+,i,i} \quad (8)$$

First, we assume that $p_{+,i,i}/p_{+,i,i-1} = 1 - \delta$, Equation (8). From this assumption, we derive the following:

$$p_{+,i,i+b_+}/p_{+,i,i} = \frac{1 - \delta - \eta}{(1 - \eta)(1 - \delta)} \quad (9)$$

By applying the conditions $0 < \delta < 1/(b_+ + 1)$ and $\eta > 1.0 - \delta$, we can further bound the expression in Equation (9) as follows:

$$p_{+,i,i+b_+}/p_{+,i,i} < (1 - \delta)^{b_+}. \quad (10)$$

Equation (10) proves that p_{+,s_i,s_j} decays at a rate faster than $(1 - \delta)$ as j increases. Consequently, the SD p_τ also decays faster than $(1 - \delta)$.

To establish **the lower bound**, we can utilize the constraint $\sum_{j \leq i} \hat{\mathcal{P}}_\tau(s_{i+1}|s_j) > \epsilon$ and construct a worst-case transition matrix as follows:

$$\forall s_i \text{ with } n_s - 1 > i > b, \mathcal{P}_-(s_{i-b_-}) \equiv 1 - \epsilon, \mathcal{P}_-(s_{i+1}|s_i) \equiv \epsilon, \mathcal{P}_-(\cdot|s_i) \equiv 0 \text{ for other cases.}$$

By analyzing this construction, we can validate that p_{-,s_i,s_j} decays at a rate slower than ϵ when j increases. Consequently, the SD p_τ also decays slower than ϵ . This completes the proof of Theorem 1. \square

Theorem 1 guarantees two critical properties. Firstly, the transition kernel remains irreducible, preventing isolated states. Secondly, it ensures that the states are increasingly difficult to reach as j increases, akin to the concept of ‘‘higher-hanging fruits.’’

While this theoretical bound provides valuable non-triviality guarantees, it remains inherently conservative due to the analytical challenges posed by randomly generated task structures. Empirically, we observe that setting $b_+ \leq n_s/4$, $b_- \geq n_s/2$, $\epsilon > 1.0e - 3$, $\eta > 0.5$ is enough to consistently yield high-quality Markov chain formulations.

Composite reward function: The reward function is designed to ensure that the value function increases progressively from low-valued states to high-valued states (in the direction of increasing j in $S = [s_1, s_2, \dots, s_{n_s}]$). Specifically, $\mathcal{R}(s, a, s')$ is composed of the following three components:

- Randomly sampled state-action dependent reward function $r_{sa}(s, a)$.
- Randomly sampled potential-based reward function $v_s(s) - v_s(s')$. This can be interpreted as a form of random reward shaping.
- State-wise reward function $r_s(s')$, which is monotonically increasing with j . This is the most crucial reward function for distinguishing high-value states from low-value states.

To ensure non-trivial task formulations, we implement a suite of validation checks. A critical safeguard involves enforcing a minimum threshold on the **normalized entropy** $\mathcal{H}(p_\sigma)$ of the SD under the oracle policy σ . For the oracle policy that might end up in absorbing states, this constraint prevents degenerate solutions to a single high-value state.

B.2 Supplementary Empirical Study on AnyMDP

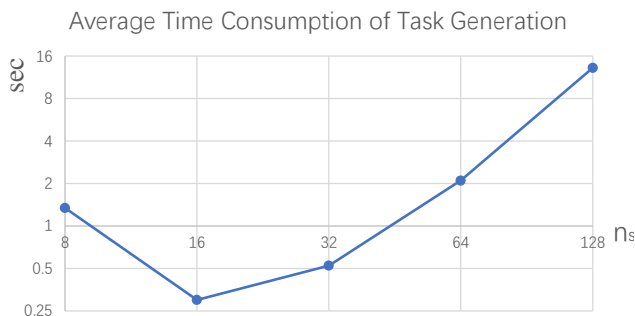


Figure 8: Time consumption of AnyMDP task generation on an Intel(R) Xeon(R) Platinum 8374C CPU.

Figure 8 illustrates the computational cost of generating AnyMDP tasks for various state space sizes $n_s \in \{8, 16, 32, 64, 128\}$. Notably, $n_s = 8$ exhibits significantly higher computation times. This is primarily due to the frequent resampling required when the value function check fails. It is important to note that the AnyMDP task generation process was executed on single CPU. Given this, the use of readily available parallelization techniques could significantly accelerate task generation.

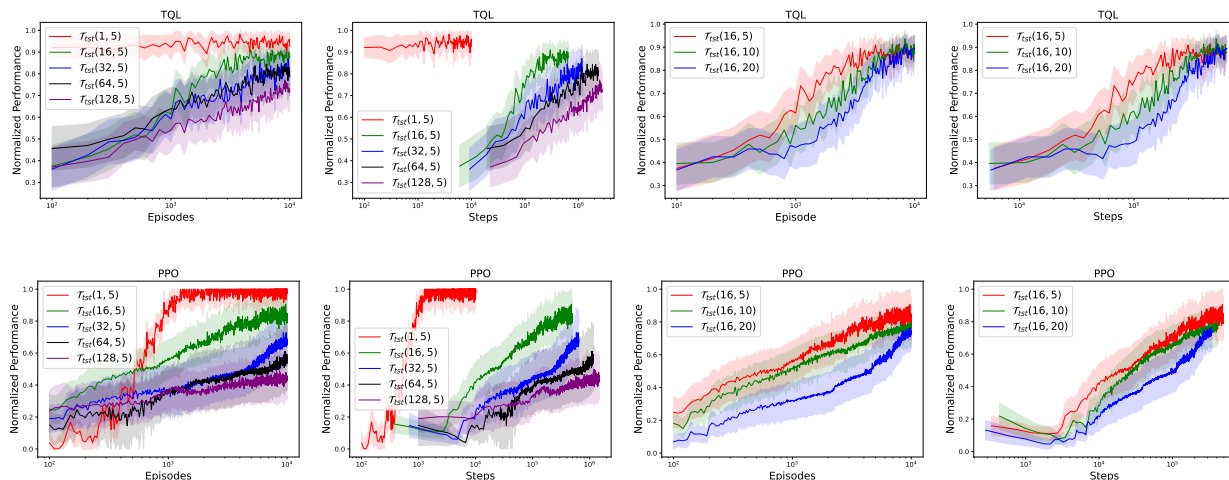


Figure 9: Performance of Tabular Q-Learning and PPO on AnyMDP tasks of variant state space and action spaces, with respect to episodes and steps.

Figure 9 illustrates the performance of Tabular Q-Learning and Proximal Policy Optimization (PPO) on AnyMDP tasks with varying state space and action space sizes. The results indicate that increasing either the state space size (n_s) or the action space size (n_a) enhances the complexity of the task, as evidenced by the need for more training steps to achieve convergence. OmniRL’s result on AnyMDP tasks with different state spaces also supports this phenomenon, shown in Figure 10. Additionally, an increase in the state space size (n_s) leads to a higher number of steps per episode.

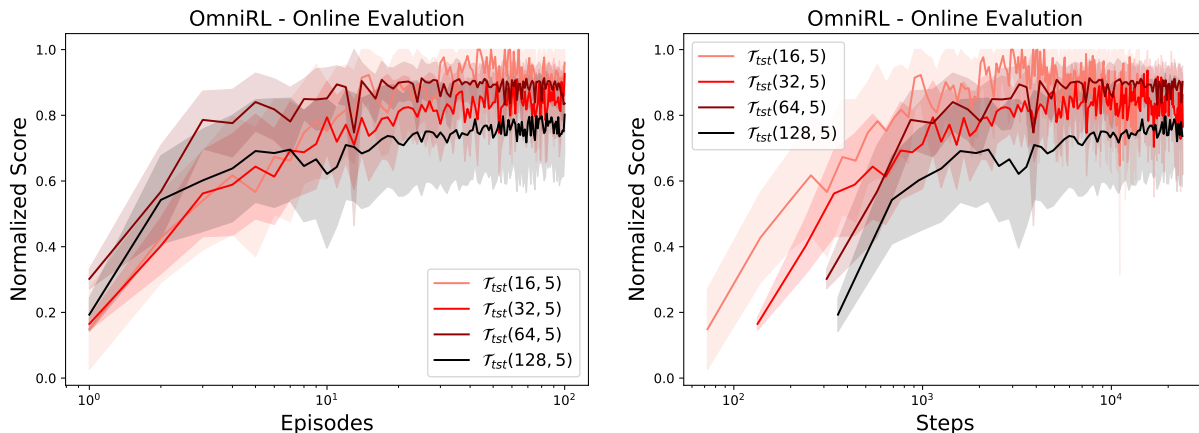


Figure 10: Performance of OmniRL on AnyMDP tasks of variant state space, with respect to steps.

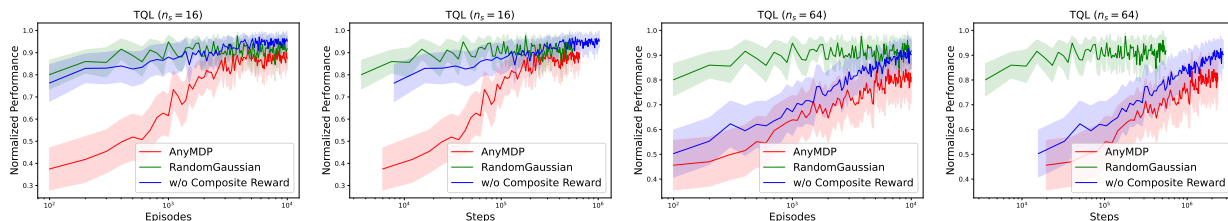


Figure 11: An ablation study comparing AnyMDP tasks with tasks sampled using other methods demonstrates that the procedural generation algorithm (Algorithm 1) produces tasks of higher quality.

Figure 11 compares three types of tasks: tasks sampled from Algorithm 1, tasks where $\langle \mathcal{P}, \mathcal{R} \rangle$ are directly sampled from naive Gaussian distributions, and AnyMDP tasks without composite reward (where \mathcal{R} is sampled from a Gaussian distribution). The results demonstrate that AnyMDP tasks provide greater challenges for reinforcement learning mechanisms.

B.3 Visualizing Discrete MDPs

Following the previous analysis, for any discrete Markov Decision Process (MDP), we can rearrange the states such that the SD p_τ decreases monotonically. We then plot the transition kernel P_τ in this rearranged order. In the visualization, we use varying opacity to represent the elements of P_τ and different colors to distinguish the initial states \mathcal{S}_0 , positively rewarded terminal states (goals) \mathcal{S}_E^+ , and negatively rewarded terminal states \mathcal{S}_E^- . This visualization, shown in Figure 12, enables us to analyze both procedurally generated AnyMDP tasks and human-designed Gymnasium tasks. Several interesting observations can be made:

- **Higher rewards for higher effort.** Both procedurally generated AnyMDP tasks and human-designed Gymnasium tasks exhibit a negative correlation between the SD p_τ and the value function V^* . This suggests a common principle: states with lower SD probability tend to have higher value functions, akin to the concept of "high hanging fruit".
- **Banded transition kernel.** When ordered by decreasing SD probability, the transition kernels of all Markov chains display the characteristics of a banded matrix. This observation further validates the effectiveness of the procedural generation method outlined in Algorithm 1.

C Details of Experiment Settings

C.1 Data Synthesis

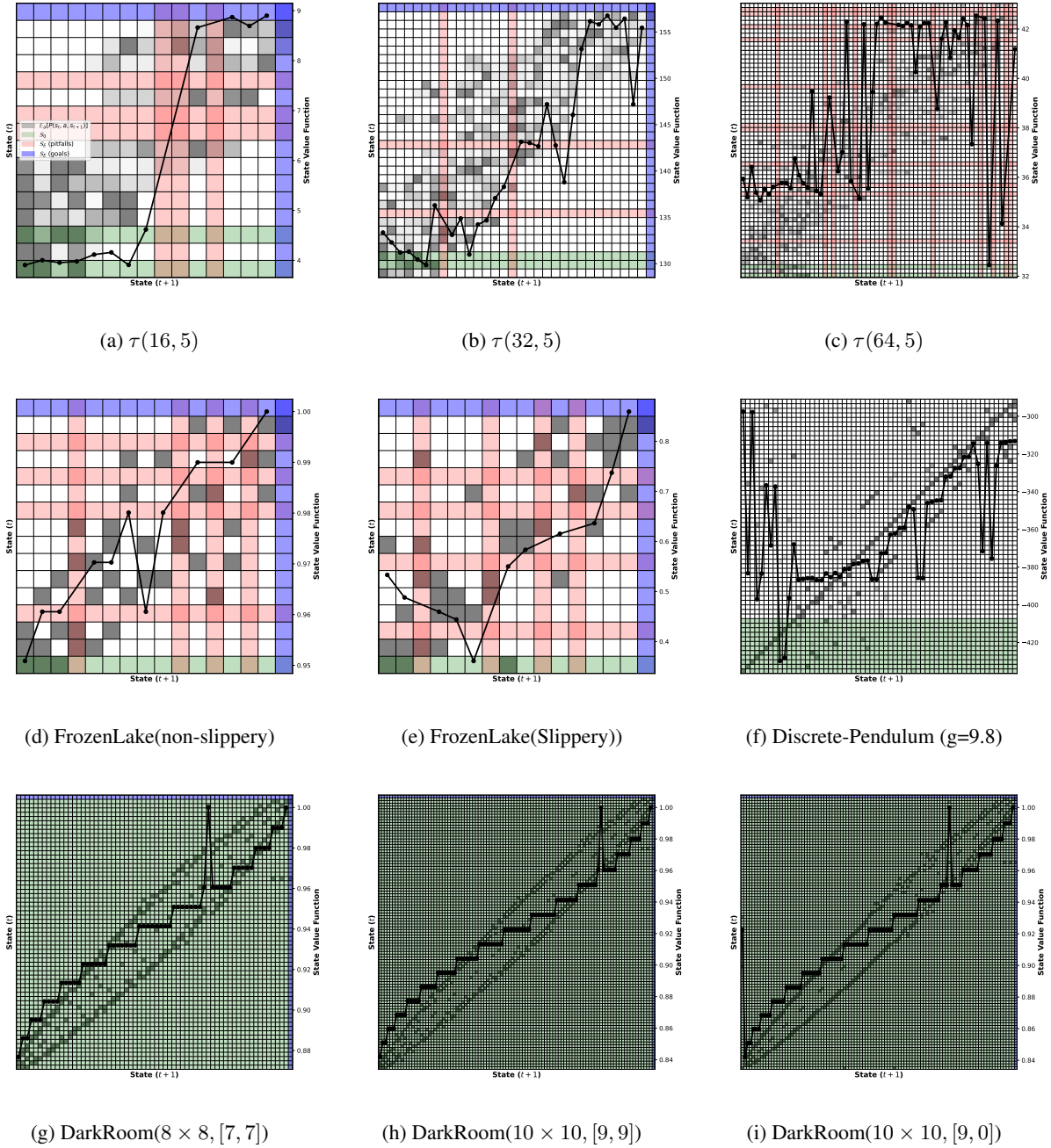


Figure 12: This figure visualizes three tasks sampled from AnyMDP, with the number of states n_s varying across $\{16, 32, 64\}$, Gymnasium tasks: non-slippery and slippery *FrozenLake* and *Discrete-Pendulum*, and 3 tasks sampled from *DarkRoom* with different dimension and goals. States are reordered according to the SD of p_τ , ordered from high to low. Gray blocks indicate state transition kernels. Red and blue blocks mark pitfalls (S_E^-) and goals (S_E^+), respectively, which trigger episode termination. Green blocks mark S_0 . The black line denotes the state value function under the optimal policy $V^*(s)$. Notably, AnyMDP is capable of generating a diverse range of tasks, including those with and without pitfalls and goals. The visualizations demonstrate that tasks generated by AnyMDP can be of comparable quality to those designed by humans. A common principle observed is that higher rewards are often associated with more challenging goals, akin to the concept of “high-hanging fruit”.

Algorithm 2 Data Synthesis Pipeline

```

Input:  $\mathcal{T}$ ,  $N_{sample}$ , Collection of behavior policies  $\Pi$ , reference policy  $\pi^*$ 
set:  $\mathcal{D}(\mathcal{T}) = \emptyset$ 
for  $[1, N_{sample}]$  do
  sample: task  $\tau \sim \mathcal{T}$ 
  set:  $t = 0, h_0 = [], l_0 = []$ 
  repeat
    sample: behavior policy  $\pi^{(b)} \sim \Pi$ 
    reset:  $\tau$  and update  $s_t$ 
    repeat
      sample:  $a_t \sim \pi^{(b)}(a|s)$ ,  $g_t = tag(\pi^{(b)})$ 
      sample:  $a_t^* \sim \pi^*(a|s)$ 
      execute:  $a_t$  in  $\tau$  and obtain  $s_{t+1}, r_t$ 
      set:  $h_t = h_{t-1} \oplus [s_t, g_t, a_t, r_t]$ ,  $l_t = l_{t-1} \oplus a_t^*$ ,  $t = t + 1$ 
    until Episode is over
  until  $t \geq T$ 
  Set:  $\mathcal{D}(\mathcal{T}) = \mathcal{D}(\mathcal{T}) \cup \{h_T, l_T\}$ 
end for
Return:  $\mathcal{D}(\mathcal{T})$ 

```

Table 4: Summarizing the data synthesis strategies of different ICRL methods.

DATA SYNTHESIS PIPELINE	BEHAVIOR POLICIES (Π)	REFERENCE POLICY
AD [12]	q	q
AD $^\epsilon$ [14]	σ^ϵ	σ^ϵ
DPT [15]	σ, q, τ	σ
OMNIRL (OURS)	$\sigma, q, m, \tau, \sigma^\epsilon$	σ

The data synthesis pipeline of OmniRL involves generating diverse trajectories h using a variety of behavior policies and creating step-wise labels l with an oracle policy π^σ . This pipeline is detailed in Algorithm 2. We incorporate at least five distinct types of agents:

- An agent with the oracle policy (σ),
- An agent with a randomized policy (τ),
- A tabular Q-Learning agent (q),
- A model-based reinforcement learning agent (m),
- An agent with the oracle policy perturbed by a decaying noise ϵ (σ^ϵ).

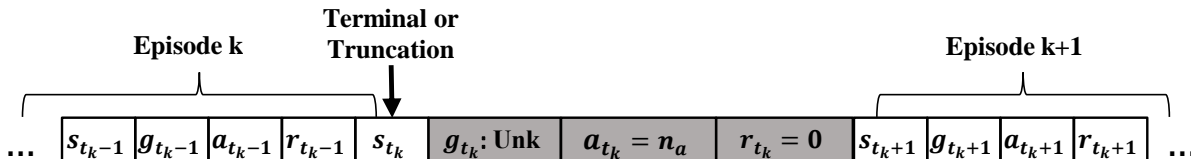
With these notations, Table 4 can be used to represent not only the data synthesis pipeline of OmniRL but also the previous imitation meta-training-based ICRL methods, including AD, AD $^\epsilon$, and DPT, as shown in Table 4. Notably, the synthesis pipeline of OmniRL is most similar to that of DPT. However, there are key differences: OmniRL employs a more diverse set of behavior policies and incorporates step-wise supervision (SS).

For the prior information g , we assign eight different IDs to the actions with $g \in [0, 7]$ which originated from 8 types of different agents, as shown in Table 5. Specifically, we exclude the actions generated by the seven types of different agents and reserve $g = 7$. This reserved ID is used to replace the action ID approximately 15% of the time steps with the data synthesis pipeline of Algorithm 2.

Addressing terminal states: The presence of terminal and truncation states necessitates special handling in reinforcement learning. In OmniRL, we avoid explicitly adding a terminal or truncation token to the sequence. Instead, we encode terminal and truncation states by introducing an additional action a , which is maintained as distinct from the standard action space \mathcal{A} . Additionally, we assign a reward of 0 and set the prior information $p = 7$ for these special steps, as depicted in Figure 13.

Table 5: Correspondance of prompt IDs and the policies it represents.

ID (g)	AGENT TYPE	DESCRIPTION
0	$\sigma(\gamma = 0)$	SINGLE-STEP GREEDY
1	$\sigma(\gamma = 0.5)$	MYOPIC GREEDY
2	$\sigma(\gamma = 0.93)$	SHORT-TERM ORACLE
3	σ	ORACLE WITH $\gamma > 0.99$
4	m	MODEL-BASED REINFORCEMENT LEARNER
5	q	TABULAR Q LEARNER
6	τ	RANDOMIZED POLICY (INCLUDING PERTURBED ACTION IN σ^ϵ)
7	UNK	RESERVED ID

Figure 13: A sketch of the tokens used to denote the intervention between two episodes. An extra action token is introduced, which is distinct from the normal actions ($a_{t_k} = |\mathcal{A}| = n_a$).

C.2 Meta-Training Details

Model structures: Before injection into causal models, the states (s_t) and actions (a_t) are encoded using embedding layers with a hidden size of 512. The rewards (r_t) are treated as continuous features encoded by 1×512 linear layer. The sequence model has a hidden size of 512, inner hidden size of 1024, hidden ratio of 2, and block number of 18 for RWKV-7. The model has approximately 43.6M total parameters (42.9M in RWKV-7 blocks), as shown in Table 6. We employ the open-source implementation of *flash-linear-attention*[†].

Table 6: The parameter settings of the sequence model. Note that for different models, the relationship between head dimension, head number, and hidden size varies. We follow the settings used in *flash-linear-attention*.

	GDN	GSA	Mamba2	RWKV7
Block nums	18	18	18	18
Hidden size	512	512	512	512
Inner hidden size	2×512	2×512	2×512	2×512
Head nums	8	8	8	8
Head dim	48	64	128	64
Parameters	46.3M	42.9M	31.6M	42.9M

Meta-training: Algorithm 3 outlines the detailed process of the meta-training procedure. Notably, we perform the backward pass segment-wise and accumulate the gradients. The gradients are not applied until the end of a sequence. We utilize a constant segment length $T_{k+1} - T_k = 2K$, which results in six backward passes for $T = 12K$ before applying the gradient.

Table 7 provides an overview of the primary datasets used in this study. For the $\mathcal{D}_{\text{Large}}$ dataset, the state space size n_s is uniformly sampled from the range [16, 128] to ensure robustness across varying state spaces. To evaluate the extrapolation capability of the model trained on $\mathcal{D}_{\text{Large}}$, we conducted a validation test with a context length of 1 million steps and observed that the loss began to gradually increase beyond 80K steps. Building upon this observation, we incorporated a post-training stage for long sequences with a context length of 512K, the dataset is denoted as $\mathcal{D}_{\text{Long}}$.

C.3 Evaluation Details

As shown in Algorithm 4, since the episode length and baseline average episodic reward vary significantly across different tasks, we normalize the episodic reward using the oracle policy (σ) and the uniform random policy (τ). This

[†]<https://github.com/fla-org/flash-linear-attention>

Algorithm 3 Meta-Training Process

Input: $\mathcal{D}(\mathcal{T}_{tra}), \mathcal{D}(\mathcal{T}_{tst})$
for epochs from 1 to maximum epochs **do**
 for $h_T, l_T \in \mathcal{D}(\mathcal{T}_{tra})$ **do**
 set: segments $K = T/T_{seg}$, gradients $g = \mathbf{0}$, initial memory $\phi_0 = 0$
 for $k \in [0, K)$ **do**
 forward: update $\phi_{k-1} \rightarrow \phi_k$ based on Equation (5), $\phi_{k-1}, h_{T_k:T_{k+1}}$ and $l_{T_k:T_{k+1}}$
 backward: calculating $g_k = \nabla \sum_{t \in [T_k, T_{k+1}]} w_t \mathcal{L}_t$ by stopping gradient of ϕ_{k-1}
 accumulate gradient: $g = g + g_k$
 end for
 apply gradient: g to update θ
 end for
 validate: averaging \mathcal{L}_t and \mathcal{L} on $\mathcal{D}(\mathcal{T}_{tst})$
end for

Table 7: Details of the meta-training dataset

DATASET	DESCRIPTION	TIME STEPS
\mathcal{D}_{Small}	$n_s = 16, n_a = 5$ $ \mathcal{T}_{tra} = \mathcal{D}(\mathcal{T}_{tra}) = 128K, SequenceLength = 8K$	$1B$
\mathcal{D}_{Large}	$n_s \in [16, 128], n_a = 5$ $ \mathcal{T}_{tra} = \mathcal{D}(\mathcal{T}_{tra}) = 512K, SequenceLength = 12K$	$6B$
\mathcal{D}_{Long}	$n_s \in [16, 128], n_a = 5$ $ \mathcal{T}_{tra} = \mathcal{D}(\mathcal{T}_{tra}) = 12K, SequenceLength = 512K$	$6B$

normalization represents the percentage of oracle performance achieved. For AnyMDP, the evaluation averages the performances over 64 variant unseen tasks. For Gymnasium tasks, the evaluation is conducted by averaging the results over 3 runs on the same task.

By default, the normalized performance S^{eval} is averaged across tasks with identical $N_{episodes}$. The deviation is estimated using the 95% confidence interval of the mean.

Algorithm 4 Evaluation Process

Input: \mathcal{T}_{tst} , collection of demonstration trajectories $\mathcal{H}_0 = \{h_0\}$,
set: $S^{eval} = \emptyset$
for $\tau \in \mathcal{T}_{tst}$ **do**
 set: R_{max} =average episodic reward of \mathbf{o} , R_{min} =average episodic reward of \mathbf{r}
 set: $S_{\tau}^{eval} = []$
 repeat
 retrieving: h_0 from \mathcal{H}_0 according to τ
 reset: τ and obtain $s_1, R = 0$
 repeat
 sample: $a_t \sim p_t^{\theta}$ with Equation (3)
 execute: a_t in τ and obtain s_{t+1}, r_t
 set: $h_t = h_{t-1} \oplus [s_t, g_t, a_t, r_t]$ with $g_t = \text{“Unk”}$
 set: $R \leftarrow R + r_t, t \leftarrow t + 1$
 until Episode is over
 calculate: normalized performance $S_{\tau}^{eval} \leftarrow S_{\tau}^{eval} \oplus [\frac{R - R_{min}}{R_{max} - R_{min}}]$
 set: $N_{episodes} \leftarrow N_{episodes} + 1$
 until $N_{episodes} > N_{max}$
 Record: $S^{eval} \leftarrow S^{eval} \cup S_{\tau}^{eval}$
end for
Return: S^{eval}

$$\begin{aligned} \text{reward} &= \begin{cases} 1, & \text{if reach goal} \\ -1, & \text{if reach hole} \\ 0, & \text{otherwise} \end{cases} & \text{reward} &= \begin{cases} 1, & \text{if reach goal} \\ -1, & \text{if reach hole} \\ -0.05, & \text{otherwise} \end{cases} \\ \text{(a) FrozenLake-v1(slippery)} & & \text{(b) FrozenLake-v1(not slippery)} & \\ \\ \text{reward} &= \begin{cases} 1, & \text{if reach goal} \\ -1, & \text{if reach cliff} \\ -0.03, & \text{otherwise} \end{cases} & \text{reward} &= \max\left(\frac{\text{reward}}{30} + 0.1, -0.1\right) \\ \text{(c) CliffWalking-v0} & & \text{(d) Pendulum-v1} & \\ \\ \text{agent reward} &= \begin{cases} 1, & \text{if reach goal} \\ 0.08, & \text{if distance to goal decrease} \\ -0.12, & \text{if distance to goal increase} \\ -0.04, & \text{if still} \\ 0, & \text{if finish} \end{cases} & & \\ \\ \text{shared reward} &= \sum_{i=1}^2 \text{agent reward}_i & & \\ \text{(e) Switch} & & & \end{aligned}$$

Figure 14: Reward shaping

For Tabular Q-Learning and PPO, we conduct 5 episodes of testing after every 100 episodes of training for each run. We evaluate performance based solely on these test episodes. In contrast, for ICRL, we do not differentiate between training and testing phases.

When performing online inference with OmniRL, we do not employ any additional exploration strategies. Instead, we maintain a softmax sampling temperature of 0.5. For offline learning, where demonstrations from the teacher are encoded, we use the original prior information g_t without modification. In contrast, for online learning, where actions are generated by the agent itself, we set $g_t = 7$ (Unk).

We apply some reward shaping to Gymnasium tasks as shown in Figure 14. OmniRL supports $n_s \leq 128$ and $n_a \leq 5$. For environments with $n_a < 5$, we find directly setting $a = a \bmod n_a$ is enough, which also demonstrates the generalizability of OmniRL to variant action spaces.

D Additional Empirical Results

D.1 OmniRL validations

OmniRL achieves automatic trade-off between exploration and exploitation. Previous studies have noted that in-context reinforcement learning (ICRL) can automatically balance exploration and exploitation. This phenomenon has been theoretically linked to posterior sampling. In Figure 15, we illustrate the entropy of the decision-making process as a function of steps within the context. When compared to Section 4.1, we observe that the decrease in loss (\mathcal{L}_t) is primarily driven by the reduction in the entropy of the policy. Specifically, the agent initially assigns equal probabilities to all actions, reflecting an exploratory phase. As more contextual information accumulates, the agent gradually converges its choices, thereby transitioning towards exploitation. This empirical finding suggests that imitating an optimal policy (oracle) is sufficient to achieve an automatic balance between exploration and exploitation.

D.2 Additional Evaluation on Gymnasium

Figure 16 and Figure 17 demonstrate OmniRL’s online-RL, offline-RL, and imitation learning capabilities toward diverse unseen tasks.

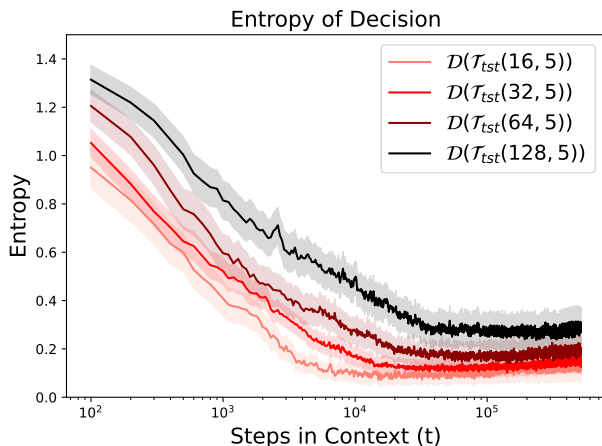


Figure 15: The position-wise entropy when validating RWKV-7 on different datasets.

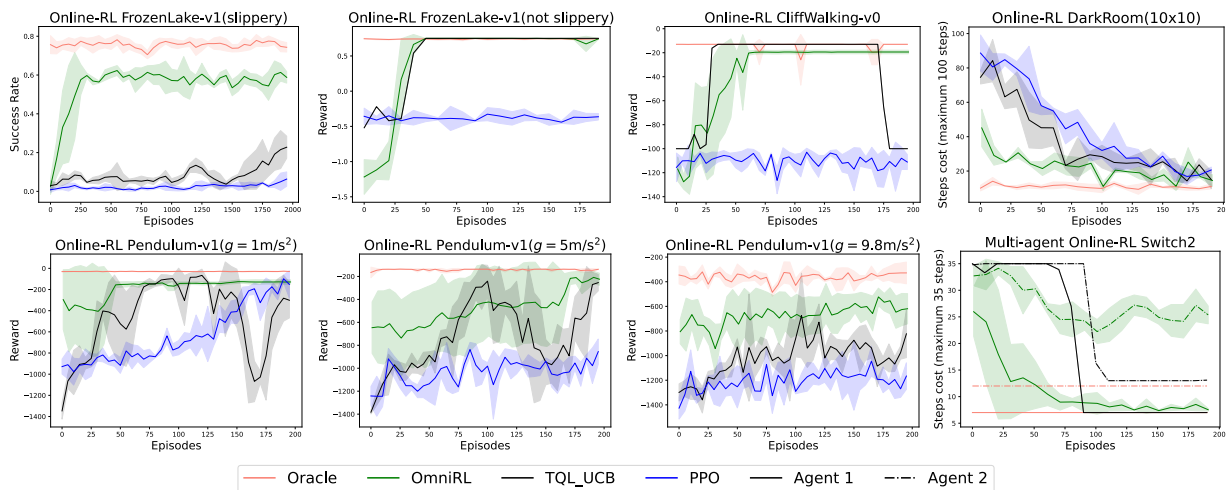


Figure 16: Selected online evaluation results for TQL-UCB, PPO, and OmniRL across Gymnasium environments. Notably, despite never having been exposed to these environments during training, OmniRL demonstrates strong adaptability by achieving competitive performance on most tasks with high sample efficiency.

D.3 Can mainstream LLMs do ICRL?

We also investigate whether a well-pretrained LLM can naturally solve the mentioned. To circumvent the lack of common sense in AnyMDP tasks, we primarily conducted tests in the *FrozenLake* task with *DeepSeek-R1*[76] in two modes:

1. Similar to the evaluation of standard ICRL, we do not provide the agent with the map. Instead, we report only the state ID and reward of the agent. The initial prompts used to initiate the evaluation are shown in Figure 18.
2. We initially provide the global map to the *DeepSeek-R1* and then commence the interaction. In this mode, the LLM can leverage the global map to make decisions. The prompts are shown in Figure 19 and Figure 20

As shown in Table 8 and Figure 23 (results executed by following the responses of DeepSeek-R1 (version 2025/03) in Figure 21 and Figure 22), LLM agents are only able to solve the *FrozenLake (non-slippery)* environment when provided with a global map. Without access to a global map, we conducted extensive interactions between LLM agents and the environment, running up to 500 episodes (100,000 steps). Despite these efforts, the agents failed to solve even the non-slippery variant of the task, achieving scores that were comparable to those of a random policy.

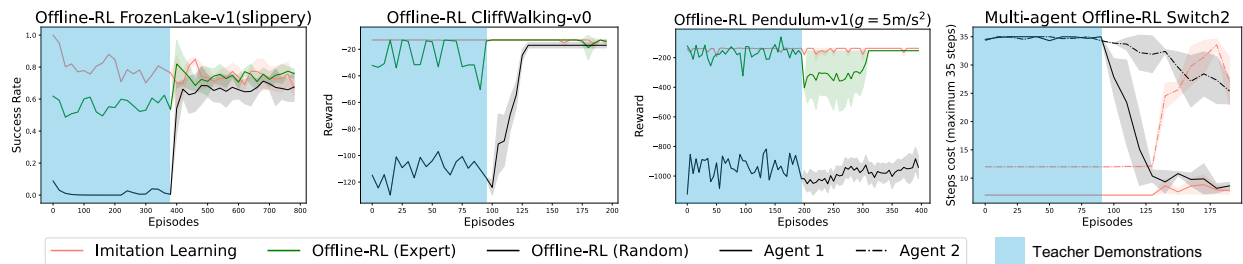


Figure 17: Selected offline evaluation results for OmniRL across Gymnasium environments, demonstrating the model’s offline-RL and imitation learning capabilities toward unseen tasks.

You are playing the Frozen Lake game. The environment is a 4x4 grid where you need to maximize the success rate by reaching the goal (+1) without falling into holes (-1). You can move in four directions: left, down, right, and up (represented as 0, 1, 2, 3 respectively). You will receive the current state and need to provide the optimal action based on your learning. When asked for the optimal action, your response must be an integer ranging from 0 to 3, and no other context is permitted. There are two kind of request types:

- integer: the integer is the current state, and you need to provide the optimal action.
- list: The list contains one or more tuples, where each tuple contains the last state, action taken, reward received, and next state. To save time, you don’t need to respond when receiving a list.

You will play the game multiple times. A game ends when the reward is -1 or 1, try to get a higher success rate.
 Note: I am asking you to play this game, not to find a coding solution or method.
 You will be provided with a conversation history. The latest prompt is the current state, and others are the list of sequential environment feedback history in tuple type. Each tuple contains four values, the first one is state, the second one is action, the third one is reward and the fourth one is next state.
 Your response must be an integer from 0 to 3 during the entire chat.
 If you find the last state is equal to the next state, your policy in the last state can’t be this action.
 If you find the reward in the tuple is -1, your policy in the last state can’t be this action.
 You need to get to the goal as soon as possible.

Figure 18: Prompts for LLM to initialize the Lake4 × 4 (Slippery) task without a global map

Even with the aid of a global map, the performance of LLM agents on the *FrozenLake (non-slippery)* environment remains notably poor. To improve their performance, we introduced additional hints suggesting that a better solution should prioritize avoiding holes over reaching the goal. However, this intervention only marginally improved the agents’ performance, raising it from 5.6% to 17%. This level of performance is still significantly lower than that of the Oracle and OmniRL agents.

Notably, increasing the length of the chain of thought can potentially enhance performance when a global map is available, but it has minimal impact on performance when only the current state is considered. The former scenario emphasizes System 2 decision-making, which is characterized by rule-based and analytical thinking. In contrast, the latter scenario highlights the in-context adaptation of System 1 decision-making, which relies on continual external feedback and represents rapid, intuitive decision-making [77, 78]. We argue that future research should place greater emphasis on the latter approach.

There is a game with the following basic description and rules:

Frozen Lake involves crossing a frozen lake from the start to the goal without falling into any holes by walking over the frozen lake. The player may not always move in the intended direction due to the slippery nature of the frozen lake.

The game starts with the player at location [0,0] of the frozen lake grid world, with the goal located at the far extent of the world, for example, [3,3] for the 4x4 environment.

Holes in the ice are distributed in set locations when using a pre-determined map or in random locations when a random map is generated.

The player makes moves until they reach the goal or fall into a hole.

The lake is slippery, so the player may move perpendicular to the intended direction sometimes.

If the intended direction is to the left, the actual move may be to the left, up, or down, with the corresponding probability distribution: $P(\text{move left}) = 1/3$, $P(\text{move up}) = 1/3$, $P(\text{move down}) = 1/3$. If the intended direction is to the right, the actual move may be to the right, up, or down, with the corresponding probability distribution: $P(\text{move right}) = 1/3$, $P(\text{move up}) = 1/3$, $P(\text{move down}) = 1/3$. If the intended direction is up, the actual move may be up, left, or right, with the corresponding probability distribution: $P(\text{move up}) = 1/3$, $P(\text{move left}) = 1/3$, $P(\text{move right}) = 1/3$. If the intended direction is down, the actual move may be down, left, or right, with the corresponding probability distribution: $P(\text{move down}) = 1/3$, $P(\text{move left}) = 1/3$, $P(\text{move right}) = 1/3$. You are given a 4x4 map where:

S represents the start.

F represents the frozen surface that can be walked on.

H represents a hole; falling into it will return the player to the start.

G represents the goal.

The map is as follows:

The first row from left to right is "SFFF".

The second row from left to right is "FHFH".

The third row from left to right is "FFFH".

The fourth row from left to right is "HFFG".

Please determine the optimal policy that maximizes the success rate of safely reaching the goal from the start. The optimal policy is the intended direction at each map location, where actions 0, 1, 2, and 3 represent moving left, down, right, and up, respectively.

Note: You are not required to write code to solve this problem; instead, directly provide the optimal policy.

Figure 19: Prompts for LLM to solve Lake4 × 4 (Slippery) with global map

In this particular environment, you should focus more on strategies to avoid encountering pitfalls rather than concentrating on reaching the goal. A reevaluation of the decision-making process in this context may yield more effective outcomes.

Figure 20: Additional guide (hint) for LLM to solve Lake4 × 4 (Slippery) with global map

The optimal policy for each state (row, column) is as follows, where each cell lists the intended direction (action) that maximizes the probability of reaching the goal:

- **(0,0)**: Down (1) - **(0,1)**: Down (1) - **(0,2)**: Down (1) - **(0,3)**: Up (3) - **(1,0)**: Down (1) - **(1,2)**: Down (1) - **(2,0)**: Right (2) - **(2,1)**: Down (1) - **(2,2)**: Down (1) - **(3,1)**: Right (2) - **(3,2)**: Right (2)

Explanation: - **Top row (0,0 to 0,3)**: Prioritize moving down to avoid the risky rightward path toward holes. - **Middle rows (1,0 and 1,2)**: Move down to progress toward safer lower rows. - **Lower rows (2,0 to 3,2)**: Navigate rightward toward the goal, avoiding holes. For example, (3,1) and (3,2) move right to reach the goal directly. - **(0,3)**: Move up (intended) to bias movement leftward (safer) and avoid falling into the hole at (1,3).

Figure 21: Responses from DeepSeek-R1 for Lake4 × 4 (Slippery) with global map

The optimal policy, revised to prioritize avoiding holes, is as follows:

- **(0,0)**: Down (1) *Avoids (0,1)'s risks by favoring transitions to (1,0) or (0,1) without direct hole exposure.*
- **(0,1)**: Right (2) *Moves toward (0,2) or (1,1) (hole). While risky, all actions here have 1/3 hole risk; right progresses toward safer (0,2).*
- **(0,2)**: Right (2) *Directs to (0,3) instead of down to (1,2), which is high-risk.*
- **(0,3)**: Up (3) *Biases movement left (to (0,2)) and avoids the hole at (1,3).*
- **(1,0)**: Left (0) *Avoids 1/3 chance of moving right into (1,1) (hole). Transitions to (0,0) or (2,0) safely.*
- **(1,2)**: Right (2) *Despite 1/3 hole risk, it allows progress to (2,2) or (0,2). Left (action 0) has equal risk but less progress.*
- **(2,0)**: Up (3) *Avoids 1/3 chance of moving down into (3,0) (hole). Routes to (1,0) or (2,1).*
- **(2,1)**: Down (1) *Safely moves to (3,1) (frozen), progressing toward the goal.*
- **(2,2)**: Down (1) *Reaches (3,2), a safe step toward the goal.*
- **(3,1)**: Right (2) *Directly progresses to (3,2), then (3,3) (goal).*
- **(3,2)**: Right (2) *Final step to the goal (3,3).*

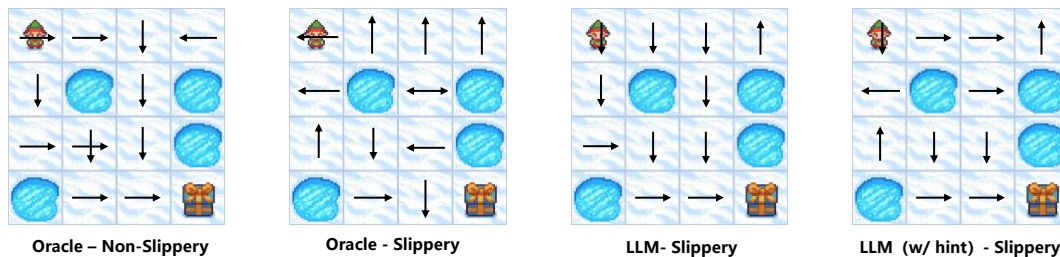
Key Adjustments from Original Policy: 1. **(1,0)**: Changed to **left** (0) to avoid 1/3 chance of falling into (1,1). 2. **(1,2)**: Changed to **right** (2) instead of down, reducing hole risk from 2/3 to 1/3. 3. **(2,0)**: Changed to **up** (3) to avoid 1/3 chance of entering (3,0). 4. **(0,1)**: **Right** (2) minimizes repeated exposure to (1,1) compared to down.

Path Safety Focus: - Avoids actions with >1/3 hole probability (e.g., down from (1,2)). - Prioritizes paths with lower immediate risk, even if longer (e.g., routing through (2,0) → (2,1) → (3,1) → goal).

Figure 22: Responses from DeepSeek-R1 for Lake4 × 4 (Slippery) with global map and hint

Table 8: Comparison of the performance (success rate) of LLM and other methods discussed in the paper within the *FrozenLake* environment.

METHODS	NON-SLIPPERY	SLIPPERY
RANDOM	1.6%	1.3%
LLM w/ STATE ONLY	< 2%	< 2%
LLM w/ GLOBAL MAP	100%	5.6%
LLM w/ GLOBAL MAP & HINT		17%
OMNIRL w/ STATE ONLY	100%	60%
ORACLE	100%	75%

Figure 23: Comparison of the solutions of different methods in the *FrozenLake* environment. In the LLM w/ hint condition, we provide additional guidance to the agent, instructing it to prioritize avoiding holes over reaching the goal.